https://doi.org/10.5194/egusphere-2025-442
Preprint. Discussion started: 12 February 2025

Insights into the Middle-Late Miocene palaeoceanographic development of Cyprus (E. Mediterranean) from a new $\delta^{18}O$ and $\delta^{13}C$ stable isotope composite record

Torin Cannings[1, 2], Alastair H. F. Robertson[1], Dick Kroon[†1]

[1]School of GeoSciences, Grant Institute, University of Edinburgh, James Hutton Road, Edinburgh EH9 3FE, UK

[2]Present address, Department of Earth Sciences, University of Geneva, Geneva, 1205, Switzerland

[†] Deceased

Correspondence to: Torin Cannings (torin.cannings@unige.ch)

Abstract. The Middle to Late Miocene was a time of significant global climate change. In the eastern Mediterranean region, these climatic changes coincided with important tectonic events, which resulted in changes in the organisation of oceanic gateways, altering oceanic circulation patterns. The Miocene Climatic Optimum is regarded as the most recent CO_2-driven warming event in Earth's climate history and has been proposed as an analogue for future climate change. We present a *c.* 12 Ma record of oxygen and carbon stable isotopes from the Island of Cyprus to help constrain the nature and extent of Miocene palaeoceanographic changes in the eastern Mediterranean region. Cyprus includes Neogene deep-sea pelagic sedimentary rocks which are suitable for stable isotope studies. Our composite geochemical record integrates data from the Lower-Upper Miocene succession at Kottaphi Hill along the northern margin of the Troodos ophiolite, and the Upper Miocene succession at Lapatza Hill to the south of the Kyrenia Range. Calcareous nannofossil biostratigraphy reveals that the composite record spans the Miocene Climatic Optimum's onset to the beginning of the Messinian Salinity Crisis. The new stable isotopic record reveals a complex interplay between global climate change and regional-to-local tectonic changes. In the earlier part of the record, global climate change dominated; however, by the end of the Late Miocene, tectonic events culminated in isolation of the Mediterranean basins, resulting in a deviation from the global open-ocean trends. Strontium isotope analysis was used primarily to help constrain the age of the Miocene successions sampled but also implies changes in the connectivity of eastern Mediterranean basins during the Late Miocene. This research provides a useful reference for oceanographic changes during the Miocene of the Eastern Mediterranean compared to the global oceans.

1. Introduction

Global climate changes during the Miocene are important analogues for modern climatic changes (You, 2010; Steinthorsdottir et al., 2021; Holbourn et al., 2022), especially as the Miocene epoch (*c.* 23-5 Ma) was a time of significant climatic and environmental changes. For the global oceans, it is currently believed that a slight cooling during the Early Miocene was

https://doi.org/10.5194/egusphere-2025-442
Preprint. Discussion started: 12 February 2025

followed by dramatic (*c.* 4°C) warming at the onset of the Miocene Climatic Optimum (MCO) at *c.* 17.9 Ma (Zachos et al., 2008; Holbourn et al., 2015; Westerhold et al., 2020). High temperatures related to the MCO ended at *c.* 14.7 Ma, during a cooling event known as the Middle Miocene Climate Transition (MMCT) (Kennett et al., 1975; Holbourn et al., 2005; Super et al., 2020). Following the MMCT, a gentle cooling trend in global temperatures continued to the end of the Miocene (Zachos et al., 2008; Westerhold et al., 2020).

However, relatively little is known about the effects of such changes more regionally, especially in marginal seas such as the eastern Mediterranean. Together with climatic changes, the eastern Mediterranean underwent tectonic changes on a regional to local scale during the Miocene, including extensive changes in the ocean circulation patterns related to the closure of several ocean gateways (Hsü et al., 1973a; Rouchy and Caruso, 2006; Robertson et al., 2012; Torfstein and Steinberg, 2020). During the Miocene, the oceanic gateway which connected the eastern Mediterranean basins with the Indian Ocean to the east was greatly restricted and eventually closed completely (Hüsing et al., 2009; Torfstein and Steinberg, 2020). The connection between the Mediterranean Sea and the Atlantic Ocean to the west was lost completely during the Late Miocene (Krijgsman et al., 1999a; Flecker et al., 2015). This resulted in the isolation of the Mediterranean Sea from the global open ocean, leading to the Messinian Salinity Crisis (MSC) (Hsü et al., 1973a; Rouchy and Caruso, 2006; Roveri et al., 2014).

Here, we present new oxygen and carbon stable isotope records from Early to Late Miocene deep-marine sediments in Cyprus, which provide an excellent reference for the eastern Mediterranean region. This new record was constructed in order to better understand the role and interplay of global climatic and regional, to local, tectonic events in the eastern Mediterranean region during the Miocene.

To understand the setting of this new record, it is important to introduce the global and regional, to local, scale changes in climate and tectonics which were important controls on sediment deposition in Cyprus during the Miocene. Therefore, in this paper, we provide an overview of Miocene palaeoceanography and tectonically-driven ocean connectivity changes together with an introduction to relevant aspects of the Miocene geology of Cyprus.

1.1 Miocene $\delta^{18}O$ and $\delta^{13}C$

Oxygen stable isotope records, mainly from deep ocean drilling, are the key to identifying and understanding important Miocene climatic events such as the Miocene Climatic Optimum (MCO) (Zachos et al., 2008; Holbourn et al., 2015; Westerhold et al., 2020). Such events are now recognised in palaeoceanographic records globally using $\delta^{18}O$ records, and more recently other methods such as Mg/Ca and organic palaeotemperature proxies (Zachos et al., 2001; Westerhold et al., 2005; Zachos et al., 2008; Holbourn et al., 2015; Modestou et al., 2020; Sosdian et al., 2020; Sosdian and Lear, 2020; Super et al., 2020; Westerhold et al., 2020).

The onset of the MCO was marked by an abrupt decrease in $\delta^{18}O$ at *c.* 16.9 Ma. This $\delta^{18}O$ trend, which is recorded in the global oceans, is associated with *c.* 4ºC increase in global temperature (Zachos et al., 2001; Westerhold et al., 2005; Zachos et al., 2008; Westerhold et al., 2020). The MCO represents a *c.* 3 Myr greenhouse interval, which began at approximately 16.9 Ma and lasted until *c.* 14.7 Ma (Zachos et al., 2008; Holbourn et al., 2015; Westerhold et al., 2020). The onset of this warming

https://doi.org/10.5194/egusphere-2025-442
Preprint. Discussion started: 12 February 2025

event is commonly attributed to a dramatic rise in CO_2 levels, from *c.* 400 ppm to 500 ppm (You et al., 2009; Zhang et al., 2013; Holbourn et al., 2015). The Middle Miocene increase in CO_2 can be explained by the rapid eruption of the contemporaneous Columbia River basalts (Hodell et al., 1994; Foster et al., 2012; Reidel, 2015; Kasbohm and Schoene, 2018). The rapid increase in $\delta^{13}C$ at *c.* 16.9 Ma indicates the onset of the Monterey Event, a positive carbon-isotope excursion, which lasted until *c.* 13.5 Ma (Vincent and Berger, 1985; Holbourn et al., 2007; Holbourn et al., 2015). The approximate co-occurrence of the MCO with the Monterey Event indicates that warming was coupled with a significant disruption of the global carbon cycle. The Monterey Event has been interpreted to represent an increase in biological carbon isotope fractionation under high CO_2 conditions, together with the enhanced burial of organic matter on continental shelves related to an eustatic sea-level rise (Vincent and Berger, 1985; Holbourn et al., 2007; Sosdian et al., 2020).

The increase in organic carbon burial related to the Monterey Event is believed to have driven CO_2 drawdown (Vincent and Berger, 1985; Flower and Kennett, 1993; Flower and Kennett, 1994; Sosdian et al., 2020), ending the MCO, and beginning the cooling event known as the Middle Miocene Climate Transition. This incorporation of CO_2 into organic material, particularly at continental margins (e.g. Monterey Formation, California, USA) (Pearson and Palmer, 2000), is believed to have resulted in a global decrease in CO_2 levels, following the highs of the MCO. Resultant increases in Antarctic bottom water and North Atlantic deep-water production, as well as a reduction in saline water movement from the Indian Ocean to the Southern Ocean (Flower and Kennett, 1994), are believed to have resulted in global-scale changes in ocean circulation that in turn triggered further cooling. This cooling event following the MCO is known as the Middle Miocene Climate Transition MMCT. According to $\delta^{18}O$-based sea-level reconstructions, the MMCT represents a dramatic three-step global cooling event, which involved three corresponding steps of extreme sea-level fall. The final temperature decrease and sea-level fall are believed to correspond to the establishment of a permanent East Antarctic Ice Sheet (EAIS) (Kennett et al., 1975; Miller et al., 1991a; Kennett et al., 2004; Holbourn et al., 2005; Miller et al., 2005).

Following the MMCT, foraminiferal $\delta^{18}O$ records indicate that global temperatures continued to cool gradually, with temperature and sea level fluctuations on the 1.2 Myr obliquity cycle (Miller et al., 2005; De Vleeschouwer et al., 2017). However, organic palaeothermometry (TEX_{86}) of samples from northern Italy (Monte dei Corvi) implies that the western Mediterranean region remained warm at the start of the Late Miocene and then cooled dramatically at *c.* 8 Ma (Tzanova et al., 2015).

The Late Miocene Carbon Isotope Shift (LMCIS) is a *c.* 1 ‰ decrease in benthic foraminiferal $\delta^{13}C$ from *c.* 7.2 to *c.* 7 Ma, probably due to a decrease in marine organic carbon burial rates. The LMCIS has been linked to the intensification of global cooling and the Asian winter monsoon during the Late Miocene (Holbourn et al., 2018). The LCMIS has been explained by changes in ocean circulation, atmospheric circulation, or a combination of other factors such as redistribution of nutrients, changes in photosynthetic pathways and terrestrial weathering (Dickens and Owen, 1999; Diester-Haass et al., 2005; Holbourn et al., 2015; Tzanova et al., 2015; Herbert et al., 2016; Lyle et al., 2019). Biogenic blooms preserved in the fossil record have also been related to the LMCIS, because the timing of the LMCIS coincides with the onset of the Late Miocene-Early Pliocene Biogenic Bloom (Dickens and Owen, 1999; Diester-Haass et al., 2004; Diester-Haass et al., 2005).

https://doi.org/10.5194/egusphere-2025-442
Preprint. Discussion started: 12 February 2025

Eustatic sea-level fall was previously inferred to be a cause of the loss of connection between the Atlantic Ocean and the proto-Mediterranean Sea, leading to the Messinian Salinity Crisis (Hsü et al., 1973a; Hsü et al., 1973b; Ryan, 1973; Adams et al., 1977; Hsü, 1978). However, benthic foraminiferal $\delta^{18}O$ records imply that sea level was relatively stable during the Messinian (Miller et al., 2020). Accordingly, it is now believed that regional to local tectonics, rather than eustasy were key to the tectonic isolation during this time (Flecker et al., 2015).

1.2 Regional tectonics and ocean gateways

Tectonic processes played an important role in the development of the eastern Mediterranean marine basins during the Miocene. During the Paleogene, the Southern Neotethys remained partly open, with the first evidence of incipient continental collision of the Eurasian and North African (Arabian) plates during the Eocene (Robertson et al., 2016; Darin and Umhoefer, 2022; Robertson and Parlak, 2024). It is likely that this initial collision resulted in a narrowing of the connection between the Southern Neotethys and the Indian Ocean by the Late Eocene (Robertson and Parlak, 2024). During the Early Miocene, the collision intensified, greatly restricting the deep-water connection with the Indian Ocean to the east. However, a marine connection through to the Atlantic Ocean to the west persisted until the Middle to Late Miocene, as indicated by palaeontological (Harzhauser et al., 2007), geological (Hüsing et al., 2009) and geochemical (Kocsis et al., 2008; Bialik et al., 2019) data. This limited connectivity still allowed warm surface water to flow from the Indian Ocean through the Mediterranean and into the Atlantic Ocean (Bialik et al., 2019).

Geological evidence (Hüsing et al., 2009; Robertson et al., 2016; Torfstein and Steinberg, 2020) and geochemical (Bialik et al., 2019; Torfstein and Steinberg, 2020) data indicate that major continental collision of the Arabian and Tauride continental crust took place during the Early Miocene (*c.* 20 Ma). This closure event left a mainly shallow seaway between the Indian Ocean and the Mediterranean Sea that finally terminated during the Late Miocene (c. 11 Ma) (Hüsing et al., 2009), in response to structural tightening of the suture zone.

During the Messinian Stage, tectonic uplift related to the northwestward migration of the African plate resulted in the closure of the Betic Straight and the Riffian Corridors (Weijermars, 1988; Garcés et al., 1998; Krijgsman et al., 1999a; Krijgsman et al., 1999b; Ng et al., 2021). The closure of these ocean gateways restricted the connection between the Mediterranean Sea and the Atlantic Ocean, as indicated by sedimentary, magnetostratigraphic and biostratigraphic data (Krijgsman et al., 1999a; Flecker et al., 2015).

As an overall result of the above tectonic events in both the west and the east, the Mediterranean Sea became isolated from the global ocean at *c.* 6 Ma, triggering the Messinian Salinity Crisis (MSC). During the MSC, Mediterranean sea level dropped at most, more than 1000m relative to the open ocean (Hsü et al., 1973a; Rouchy and Caruso, 2006). This dramatic sea-level fall and related hyper-aridity resulted in the deposition of thick evaporites across the Mediterranean area after *c.* 5.57 Ma.

https://doi.org/10.5194/egusphere-2025-442
Preprint. Discussion started: 12 February 2025

1.3 Miocene of Cyprus

The island of Cyprus is composed of three distinct geological units (terranes) (Fig. 1), each of which has a unique geological history. The Kyrenia Range in the north (Robertson and Woodcock, 1986; Robertson, 1990), the Troodos O ophiolite (Gass and Masson-Smith, 1963; Moores and Vine, 1971) in the island's centre, and the Mamonia Complex in the west (Lapierre, 1972; Robertson and Woodcock, 1979; Robertson, 1990; Robertson and Xenophontos, 1993) (Fig. 1). During the Mesozoic, the Mamonia Complex and the Kyrenia Range formed parts of the continental margin of the Southern Neotethys. During the Late Cretaceous, the Troodos ophiolite formed within the Southern Neotethys by spreading above a subduction zone. During the Paleogene, the Troodos ophiolite and the Mamonia Complex were covered by a Cretaceous to Oligocene sequence of mainly deep-water pelagic carbonates, known as the Lefkara Formation (Mantis, 1970; Robertson and Hudson, 1973; Robertson, 1976; Kähler and Stow, 1998; Lord et al., 2000). The underlying Troodos ophiolite and the Mamonia Complex significantly uplifted during the Oligocene-Early Miocene. The main drivers were the continental collision between Arabia and the Taurides to the east, and northward subduction/underthrusting beneath Cyprus (Robertson, 1998). The resulting uplift resulted in relative sea-level fall, allowing the deposition of variable shelf-depth sediments of the Lower-Upper Miocene Pakhna Formation in southern Cyprus, which includes hemipelagic carbonates, gravity-flow deposits and localised coral reefs (Robertson, 1977; Follows and Robertson, 1990; Robertson, 1990; Follows et al., 1996; Cannings et al., 2021). The stratigraphical contact between the Lefkara and Pakhna formations is likely to be variable in facies and age (Bagnall, 1960; Pantazis, 1967; Eaton and Robertson, 1993; Read, 1993).

Two reef-related members are included within the Paknha Formation. The Lower Miocene Terra Member is the stratigraphically lowermost of these units and is dominantly composed of framestones, which display high levels of algal and coral biodiversity (Follows et al., 1996; Coletti et al., 2021). The Upper Miocene Koronia Member includes a reef facies that is almost mainly composed of Poritid corals (Follows and Robertson, 1990; Coletti et al., 2021), together with off-reef facies composed of rhodolith-rich packstones, calcarenites and chalks that contain scattered bivalve and poritid fragments (Follows and Robertson, 1990). The Pakhna Formation is overlain by a suite of cyclical alterations of chalk and gypsum which are assigned to the Kalavasos Formation, and are associated with the onset of the MSC (Hsü et al., 1973b; Krijgsman et al., 2002; Wade and Bown, 2006; Manzi et al., 2016). The gypsum accumulated in several small tectonically controlled basins around the periphery of the Troodos Massif. Of particular relevance here, the Pakhna Formation includes nannofossil ooze (chalk) and planktic foraminifer-rich calcareous mudstones (marls) that were sampled for this study on the northern margin of the Troodos ophiolite.

The Miocene sedimentary succession of the northern part of the Cyprus associated with the Kyrenia Range, differs strongly from that of the southern Cyprus related to the Troodos ophiolite. The Miocene in the north encompasses an Upper Eocene Upper Miocene succession of variably deformed non-marine to relatively deep marine conglomerates, sandstones and mudstones, known as the Kythrea (Dğirmenlik) Group (McCay et al., 2013; Robertson et al., 2014; Chen et al., 2022). The Early-Middle Miocene of the Kythrea (Değirmenlik) Group is dominated by mudrocks and siliciclastic gravity-flow deposits,

https://doi.org/10.5194/egusphere-2025-442
Preprint. Discussion started: 12 February 2025

which were deposited as part of a trench or foreland basin along the northern margin of the southern Neotethys (McCay et al., 2013). By the Late Miocene, the input of sand-sized siliciclastic sediment waned allowing Tortonian mudstones and marls to accumulate along the southern margin of the range, termed the Yılmazköy Formation. With a further decrease in siliciclastic input, dominantly hemipelagic marls, associated with thin layers rich in manganese oxide, accumulated during Tortonian-Lower Messinian, termed the Yazılıtepe Formation (Robertson et al., 2019). The overall succession is capped by Messinian gypsum. known as the Lapatza (Mermertepe) Formation (Hakyemez et al., 2000; McCay et al., 2013). Marls of the Yazılıtepe Formation to the south of the Kyrenia Range were also sampled during this research.

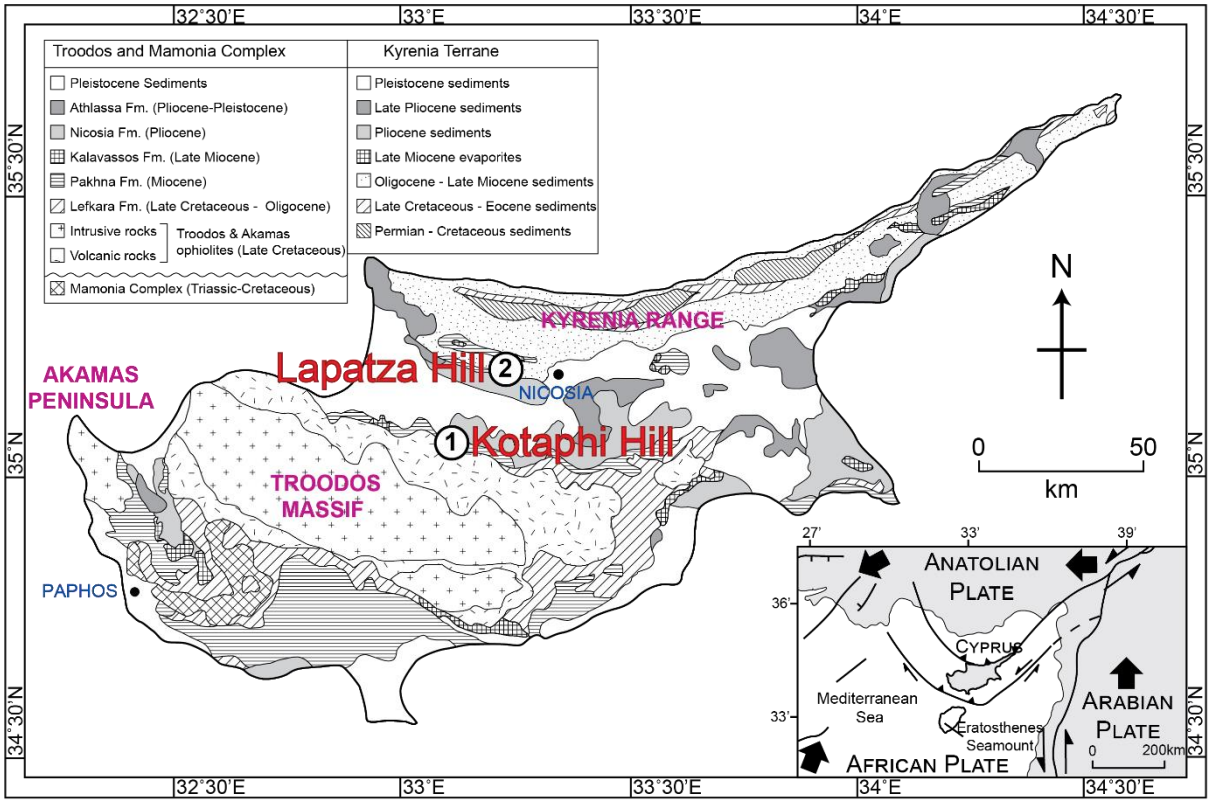

Figure 1 Outline geological map of Cyprus showing the Troodos Massif, the Mamonia Complex and the Kyrenia Range, as well as their sedimentary cover (modified from Kinnaird et al., 2011). Site locations for this study are also shown.Inset: tectonic setting of Cyprus in the eastern Mediterranean region (modified from Follows and Robertson, 1990; Robertson et al., 1991; Payne and Robertson, 1995).

2 Methods

2.1 Site selection

To ensure that the samples collected provided a continuous record of the Early-Late Miocene target time interval (*c.* 17.5 – 5.33 Ma), several exposures across the island of Cyprus were selected for logging and sampling. This included previously studied sections and several new sections that were sampled and logged for the first time. Approximate ages were available

https://doi.org/10.5194/egusphere-2025-442
Preprint. Discussion started: 12 February 2025

for the previously studied exposures, whereas the likely age range of the new sections was initially inferred mainly based on lithological correlations. The samples from the new successions were dated during this work using calcareous nannofossil biostratigraphy (Cannings, 2024). Following fieldwork and preliminary dating, two sections were selected to produce a composite succession spanning *c.* 17.5 – 5.33 Ma, one on the north side of the Troodos ophiolite at Kottaphi Hill, and the other to the south of Kyrenia Range at Lapatza Hill (Fig. 1). Other sections that proved to be less suitable for the composite succession are detailed in Cannings (2024).

2.1.1 Kottaphi Hill

Kottaphi Hill (Κοτάφι, Kotaphi or Kottafi) (35° 2'50.40" N 33° 9'13.60" E) is located to the north of Agrokipia (Αγροκηπιά) village (Nicosia District) on the northern margin of the Troodos ophiolite (Fig. 1). Kottaphi Hill is a classic Miocene section of the Pakhna Formation (Mantis, 1972) that has been the subject of several previous studies (Follows and Robertson, 1990; Davies, 2001; Penttila, 2014; Athanasiou et al., 2021; Coletti et al., 2021). The Miocene succession there (Fig. 2a & b) begins with *c.* 60m of cyclically bedded chalk and marl (i.e. couplets), which are assigned to the Pakhna Formation (undifferentiated). This pelagic-hemiplegic succession is overlain by redeposited bioclastic limestones, followed by debris-flow deposits that are dominated by neritic carbonate including Poritd corals, and assigned to the Koronia Member (Follows and Robertson, 1990; Follows, 1992).

Previously, Davies (2001) logged and sampled the Kottaphi Hill succession at a resolution of > 20 cm), with the main aim of determining the relative roles of climate versus tectonics on sedimentation. The succession was dated as Burdigalian-Tortonian using calcareous nannofossil biostratigraphy, supported by the available carbon and oxygen stable isotope records. Davies (2001) described a well-cemented trace-fossil-rich manganese and iron-rich layer roughly halfway up the succession, and inferred that this represented a hardground. Based on spectral analysis, Davies (2001) suggested that the chalk-marl cyclicity (couplets) at Kottaphi Hill was controlled by regional to global changes in climate and sea-level; i.e. Milankovitch cyclicity. Davies (2001) also identified the Monterey Excursion in the available $\delta^{13}C$ record, and linked a positive $\delta^{18}O$ trend from 13 to 14 Ma with the closure of the Mediterranean. The isolation of the Mediterranean from the Indian Ocean had previously been suggested as a reason for a positive $\delta^{18}O$ trend in the Miocene stable isotope record from Malta (Jacobs et al., 1996).

Building on Davies's (2001) study, Penttila (2014) used calcareous nannofossil biostratigraphy and strontium isotope dating, together with foraminiferal abundance and selected X-ray diffraction analysis. She identified an incoming of feldspar and clay-rich lithic fragments at *c.* 10.6 Ma and suggested that this indicated that the adjacent Troodos Massif was near or above theseafloor by this time allowing erosion of extrusive ophiolitic rocks to take place Penttila (2014) also identified 'ghost sapropels' (<2% total organic carbon) towards the top of the succession.

Subsequently, Athanasiou et al. (2021) collected samples from a 42.1 m-thick succession on the lower slopes of Kottaphi Hill. The samples collected underwent calcareous nannofossil, pollen and palynomorph, $\delta^{13}C$ and $\delta^{18}O$ and total organic carbon analysis. Athanasiou et al. (2021) inferred that the organic carbon-rich layers at Kottaphi Hill were deposited in warm

https://doi.org/10.5194/egusphere-2025-442
Preprint. Discussion started: 12 February 2025

oligotrophic seawater, with strong water column stratification, and further suggested that these layers represent the precursors to sapropels. These authors also identified the Mi3–Mi5 events (Miller et al., 1991a; Miller et al., 2020) and the CM5–CM7 episodes (Woodruff and Savin, 1985, 1991) in their $\delta^{13}C$ and $\delta^{18}O$ stable isotope record. Pollen and palynomorph analysis indicated that land nearby was densely vegetated before *c.* 14.5 Ma. After *c.* 13 Ma, a more open landscape was inferred, accompanied by nearby high rates of soil erosion.

2.1.2 Lapatza Hill

A *c.* 60m-thick succession of well-bedded, laterally continuous marls that is exposed on Lapatza Hill (Lapatza Vouno) (35°14'44.70" N 33° 8'35.80" E) (Fig. 1, Fig. 2c) is lithologically correlated with the Tortonian-Lower Messinian Yazılıtepe Formation. The succession includes numerous thin (<20 cm) manganese-rich layers (Necdet, 2002), similar to those described within the Yazılıtepe Formation in the Karpas Peninsula of NE Cyprus (Robertson et al., 2019). At Lapatza Hill, the marls are directly overlain by gypsum, which constitutes the type section of the Lapatza (Mermertepe) Formation (Henson *et al.*, 1949); this is assumed to be of Mid-Late Messinian age, as elsewhere in Cyprus (McCay et al., 2013; Varol and Atalar, 2017; Artiaga et al., 2021).

https://doi.org/10.5194/egusphere-2025-442
Preprint. Discussion started: 12 February 2025

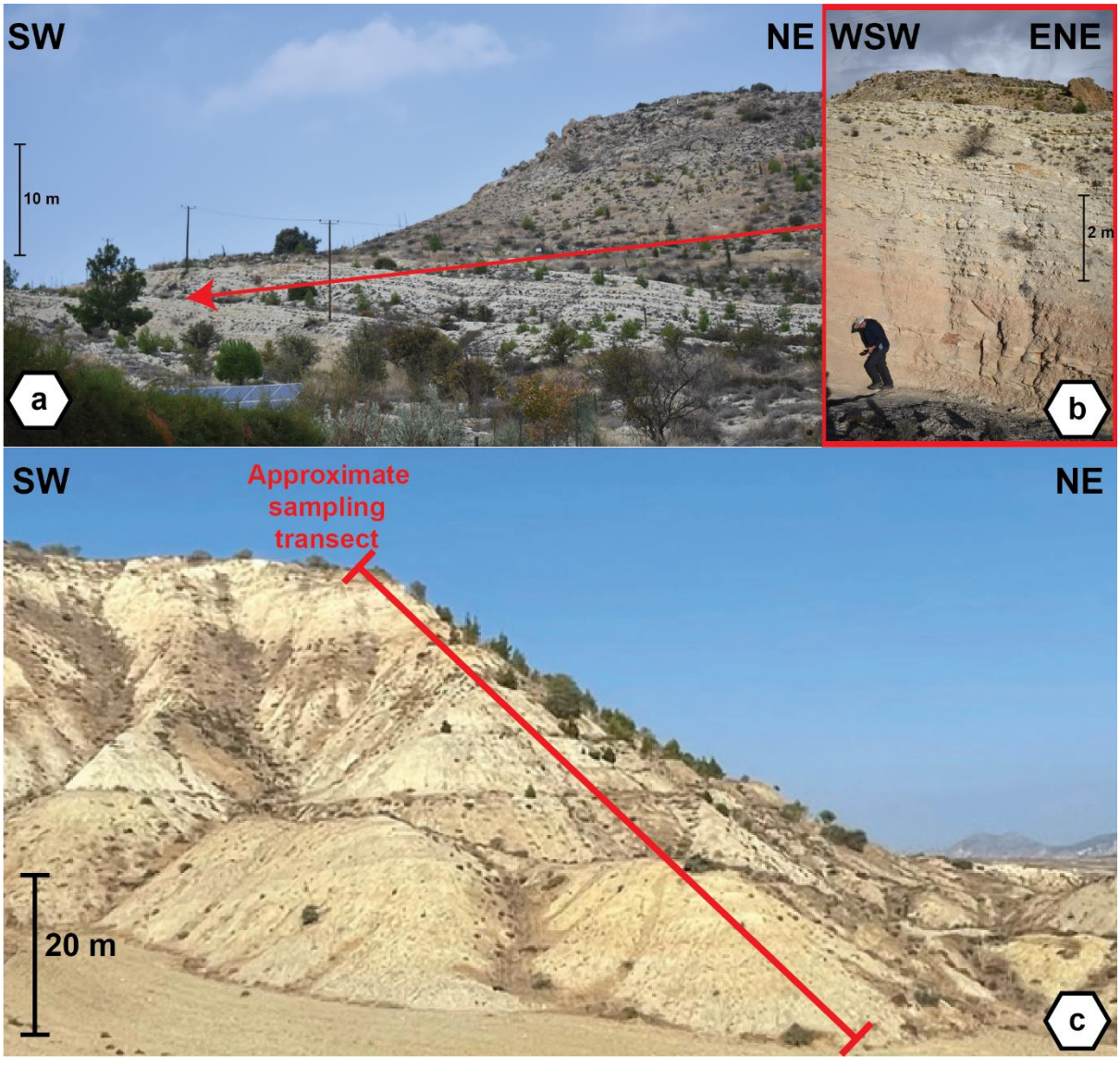

Figure 2 Photographs showing the Kottaphi Hill succession. (a) with the first interval of high-resolution sampling indicated (b), as well as the sampled succession at Lapatza Hill (c), with the approximate sampling transect indicated (red).

2.2 Sampling

Samples were collected by hand using a geological hammer and a chisel to dig out and collect sediments that were unaffected by surface processes as far as possible. A shovel was sometimes needed to excavate a trench and take samples, especially where loose sediment cover needed to be removed as at Lapatza Hill. The samples were collected at short (i.e. 5-25 cm) intervals to allow high-resolution geochemical records could be obtained. The sampling resolution varied for each locality based on the time interval covered and the inferred sedimentation rate. Previous studies indicated that the deposition of the

https://doi.org/10.5194/egusphere-2025-442
Preprint. Discussion started: 12 February 2025

sediments between 10.8 and 29.5 m in the Kottaphi Hill succession coincided with the MCO and MMCT. Therefore, this part of the succession was subjected to the highest-resolution sampling (5cm). Preliminary dating of the Lapatza Hill succession indicated a high (1-3 cm/kyr) sedimentation rate; therefore, a larger (25 cm) sampling interval was used for this interval. Sedimentary logs detailing changes in the lithology, sedimentary structures and the presence of fossils were made for both successions during the sample collection.

2.3 Foraminifera

The planktic *Praeorbulina-Orbulina* lineage (Blow, 1956; Pearson et al., 1997; Aze et al., 2011; Spezzaferri et al., 2015) was used for the geochemical analysis. The foraminiferal species within the target interval and are not known to have vary in vital effects, depth habitat or symbiotic association (Pearson et al., 1997).

Samples were washed using a 32 μm sieve to remove fine clay and silt fractions. Samples which were not easily broken up by wet sieving were soaked in Milli-Q water and placed on a shaker plate for 90 minutes before being washed again over a 32 μm sieve. This process was repeated up to 3 times for the most resistant samples. The foraminiferal samples were then dried in an oven at 30°C and dry sieved into size fractions for foraminiferal picking.

2.4 Calcareous nannofossil biostratigraphy

Calcareous nannofossil biostratigraphy has been used successfully in Cyprus in several previous studies (Morse, 1996; McCay et al., 2013; Robertson et al., 2019; Cannings et al., 2021).

Calcareous nannofossils were identified using smear slides that were prepared using the standard method (Backman and Shackleton, 1983; Bown and Young, 1998), and then examined with a light microscope at a magnification of ×1000–1250. The calcareous nannofossil biostratigraphy used here is based on Backman et al. (2012).

2.5 Strontium isotope dating

The well-established strontium isotope dating technique (Elderfield, 1986) was previously used for the dating of mainly Neogene carbonate sediments in Cyprus (McCay et al., 2013; Penttila, 2014; Cannings et al., 2021). The isolation of the Mediterranean Sea during the Messinian Salinity Crisis (MSC) is believed to have resulted in anomalous $^{87}Sr/^{86}Sr$ ratios during this time, such that samples of this age range cannot be reliably dated using this method (Flecker and Ellam, 1999; Flecker et al., 2002; Flecker and Ellam, 2006).

Five samples of planktic foraminifera from the *Praeorbulina-Orbulina* lineage from the Kottaphi Hill succession, and five samples of planktic foraminifera also from the *Praeorbulina-Orbulina* lineage from the Lapatza Hill succession were dated using the strontium (Sr) isotope method. These 10 planktic foraminiferal samples were then analyzed to help test and constrain the dating of the overall composite succession, as achieved by biostratigraphic methods. The strontium isotope analysis was carried out at the Scottish Universities Environmental Research Centre using a VG-Sector-54 thermal ionization mass spectrometer. Further details of the methodology used for strontium isotope analysis is provided in the supplementary material.

https://doi.org/10.5194/egusphere-2025-442
Preprint. Discussion started: 12 February 2025

Strontium isotopic ages were calculated using the LOWESS Sr isotope Look-Up Table (Version 4: 08/04) (McArthur et al., 2001; McArthur and Howarth, 2004). The total combined errors were calculated by combining the uncertainties of the Sr isotopic analyses, with the error of the LOWESS Sr isotope Look-Up Table (Version 4: 08/04) (McArthur et al., 2001; McArthur and Howarth, 2004).

2.6 Stable isotope analysis

Both a bulk carbonate (fine fraction ≤63 um) and a planktic foraminiferal stable isotope record are presented below for the 'composite succession' obtained from Kottaphi Hill and Lapatza Hill. The provision of both bulk carbonate (fine fraction) and planktic foraminiferal records provides the most complete isotope record possible for the target time interval, by reducing the gaps in the record to a minimum. However, bulk carbonate and planktic foraminiferal records can differ due to variable vital effects in the biogenic components (Anderson and Cole, 1975; Reghellin et al., 2015). A planktic foraminiferal sample contains only one biogenic component, whereas a bulk carbonate sample contains multiple biogenic components and also their fine-grained matrix.

For the bulk analysis, 640 samples were broken up and dry sieved through a 38 μm sieve, in order to collect a concentrated sample of nannofossil carbonate and reduce the likelihood of terrigenous components being present. The samples were then ground using a porcelain pestle and mortar to ensure a consistent/homogeneous fine powder. ~ 0.5 mg of each powdered sample was then taken for isotopic analyses. All of the stable isotope measurements of the bulk carbonate (fine fraction) samples were run in the Wolfson stable isotope ratio mass spectrometry suite at Edinburgh University on an Elementar precisION continuous flow stable isotope ratio mass spectrometer, using a Gilson autosampler equipped with an automated acidification system, heated tray and an iso FLOW system.

The isotopic measurements of 578 foraminifera samples were conducted in the Wolfson stable isotope ratio mass spectrometry suite at the School of GeoSciences at the University of Edinburgh using a dual-inlet Thermo Electron Delta + Advantage stable isotope mass spectrometer, interfaced with a Kiel carbonate II device.

2.7 Age model

New age models were generated for both the Kottaphi Hill and Lapatza Hill successions.

For each succession, a preliminary age model was created based on calcareous nannofossil biostratigraphy. Sedimentation rates were calculated based on the depth/height difference between samples identified as bio-horizons. Samples that were not biostratigraphically dated were assigned tentative ages using a linear interpolation based on the calculated sedimentation rate.

The final age model was produced using AnalySeries 2.0.8 (Paillard *et al.*, 1996). The new $\delta^{18}O_{planktic}$ record produced for this study was used for this purpose and aligned with the North Atlantic $\delta^{18}O_{benthic}$ compilation record of Cramer *et al.* (2009).

For the alignment, the new $\delta^{18}O_{planktic}$ record was filtered using multiple steps (20, 60, 100 ky) of box filtering, in order to reduce 'noise' and only reveal long-term trends and major perturbations. Identifiable marine isotope stages/events and major trends within the record were aligned with the reference record by creating tie points at the midpoints of such trends. This age

https://doi.org/10.5194/egusphere-2025-442
Preprint. Discussion started: 12 February 2025

modelling technique has uncertainty resulting from a combination of the uncertainties associated with the calcareous nannofossil biostratigraphy, the $\delta^{18}O_{planktic}$ record of this study and $\delta^{18}O_{benthic}$ target record (Cramer *et al.*, 2009).

Age models were produced separately for both the Kottaphi and Lapatza hill successions using the same method. The records were then carefully compared to identify the most suitable splice point to combine the two records to produce a composite record for the whole of the target time interval.

3 Results

3.1 Sedimentary logs

3.1.1 Kottaphi Hill

The sampled Kottaphi Hill succession begins *c.* 10 m stratigraphically below the prominent hard layer which was previously interpreted as a 'hardground' (Davies, 2001). A simplified stratigraphic log of the sampled Kottaphi Hill succession is shown in Fig. 3a (the detailed stratigraphic log of the succession is recorded in the supplementary material).

The measured succession at Kottaphi Hill begins with 10.97m of alternating beds of light buff-coloured chalk and slightly darker buff-coloured calcareous marl. At 10.97m, there is an abrupt lithological change to three hard grey limestone beds, interbedded with darker, buff-coloured micritic limestone. The upper surfaces of the three limestone beds are dominated by well-preserved trace fossils (*Thalassinoides, Diplocraterion* and *Zoophycos)*. This unit can be reinterpreted as a firmground, rather than a hardground (Cannings, 2024). Above the final micritic limestone, chalk and calcareous marl interbeds start at 11.3m. These beds have a distinct pinkish-red colour which gradually fades to a buff colour over *c.* 4m. Further up section, the abundance of chalk beds increases relative to marl beds. From 27.79m to 32.96m, thick (30-85cm) chalky marl beds are interbedded with thinner (5-20cm) marl beds. Several soft marl beds within this facies have a distinctive dark reddish-brown colour. In the field, these marl layers were interpreted as oxidised "ghost sapropels". Above this level, exposure is patchy to rare and is mostly covered by reworked debris from the above units and so was not sampled for stable isotope analysis.

3.1.2 Lapatza Hill

The succession sampled at Lapatza Hill (Fig. 3b) comprises 63.1m, mainly calcareous marl, with infrequent layers of darker brown marl, dark red marl and chalky calcareous marl. Fine parallel laminations are present throughout the succession, which become more prominent towards the top of the succession. Sedimentary structures (including observable bioturbation) are otherwise absent. This succession is abruptly overlain by a *c.* 15 m-thick interval of fine-grained alabastrine gypsum that continues to the top of the hill where the section ends.

The calcareous marls are very rich in planktic foraminifera at the base; however, at *c.* 52.5m their abundance decreases, especially in the softest marl beds. At *c.* 61m, foraminifera are completely absent. Some foraminifera occur in chalky marl beds at *c.* 62m; however, their abundance rapidly decreases towards the contact with the overlying gypsum. Additionally,

https://doi.org/10.5194/egusphere-2025-442
Preprint. Discussion started: 12 February 2025

numerous thin (1-5 cm) dark brown and red marl manganese and iron-rich layers occur within the calcareous marl sequence, although these were not sampled during this study.

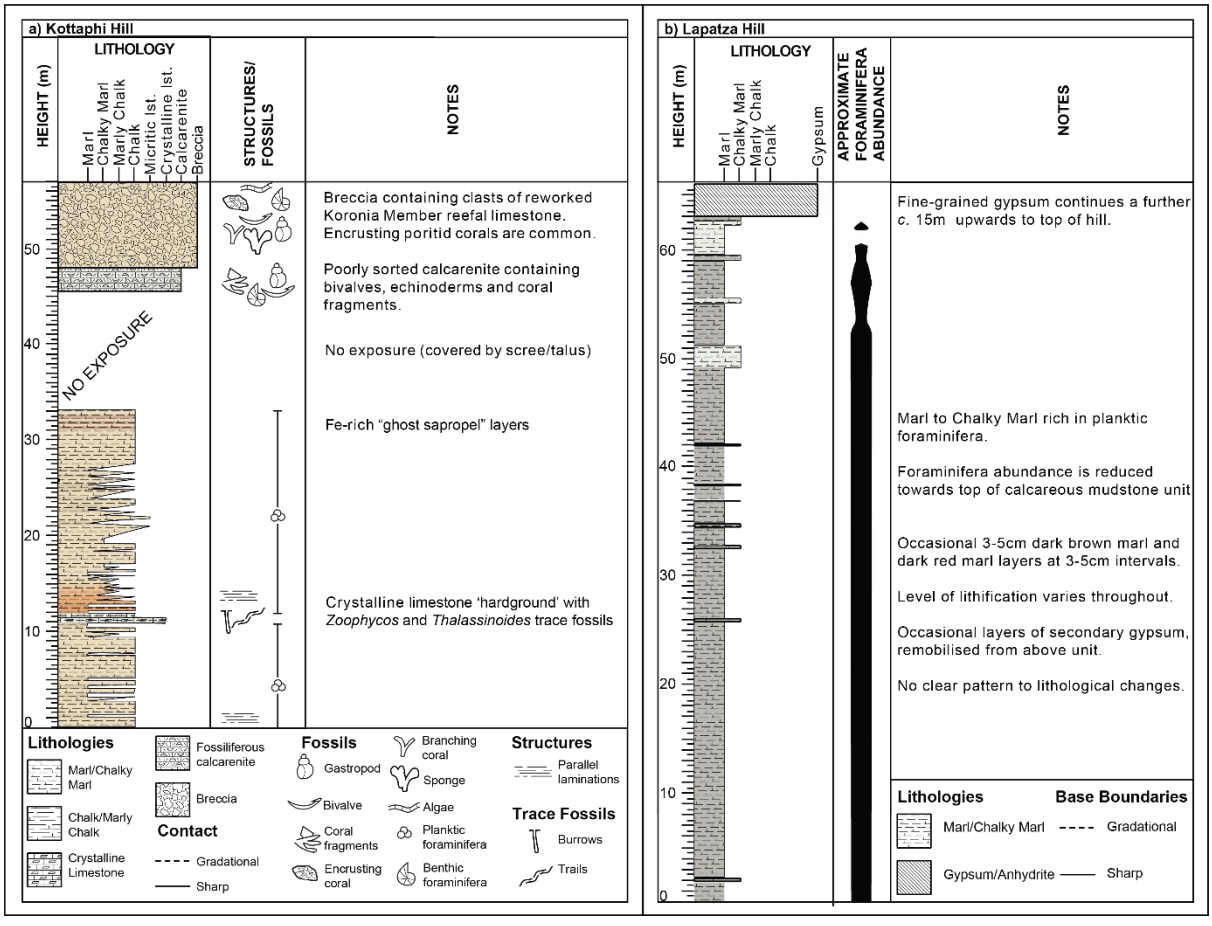

Figure 3 Simplified stratigraphic logs of the Kottaphi Hill succession (a) showing the occurrence of sedimentary structures and fossils up the section and the Lapatza Hill succession (b) showing the approximate abundance of planktic foraminifera and the main lithological changes up the succession.

3.2 Calcareous nannofossil biostratigraphy

3.2.1 Kottaphi Hill

Figure 4a shows the ages obtained using calcareous nannofossil biostratigraphy for the samples from the Kottaphi Hill succession. Accordingly, the base of the succession is between 19.01 and 17.96 Ma, as indicated by the presence of *Sphenolithus belemnos* (Backman et al., 2012). The top of the sampled succession is slightly younger than 8.8 Ma, as indicated by an increase in the relative abundance of *Reticulofenestra pseudoumbilicus* just beneath the top of the succession. These dates indicate that the Kottaphi Hill succession has an average sedimentation rate of *c.* 0.25 cm/ky. Calcareous nannofossil biostratigraphy indicates that the highest sedimentation rate was 0.33 cm/ky between 11.88 Ma and 11.60 Ma, and the lowest

https://doi.org/10.5194/egusphere-2025-442
Preprint. Discussion started: 12 February 2025

was 0.19 cm/ky between 17.75 Ma and 15.73 Ma. These sedimentation rates do not take account of diagenetic compaction, which was however, minor because there is no evidence of deep burial or deformation of either of the two successions studied.

3.2.2 Lapatza Hill

Figure 4b shows the ages inferred using calcareous nannofossil biostratigraphy for the samples from the Lapatza Hill succession. The increase in the relative abundance of *Reticulofenestra pseudoumbilicus* slightly above the base indicates that the base of the succession is older than 8.8 Ma (using the biostratigraphy of Backman *et al.*, 2012). The first occurrence of *Amaurolithus primus* at *c.* 18.5m indicates an age of 7.39 Ma. These dates indicate that the Lapatza Hill succession has an average sedimentation rate (non-decompacted) of *c.* 1.01 cm/ky. Calcareous nannofossil biostratigraphy indicates that the highest sedimentation rate was 1.08 cm/ky between 8.8 Ma and 7.39 Ma. The lowest sedimentation rate was 0.92 cm/ky between 7.39 Ma and 7.09 Ma.

The calcareous nannofossil assemblages above the 25m level in the Lapatza Hill succession are not diagnostic of age. Samples from the upper part of the section contain a diverse calcareous nannofossil assemblage; however, age-indicative species are absent. One notable observation from the calcareous nannofossil biostratigraphy of the Lapatza Hill succession is the absence of all calcareous nannofossils from the *Discoaster* genus above *c.* 60m. In contrast, *Discoaster spp.* specimens are abundant in samples from the lower part of the succession.

https://doi.org/10.5194/egusphere-2025-442
Preprint. Discussion started: 12 February 2025

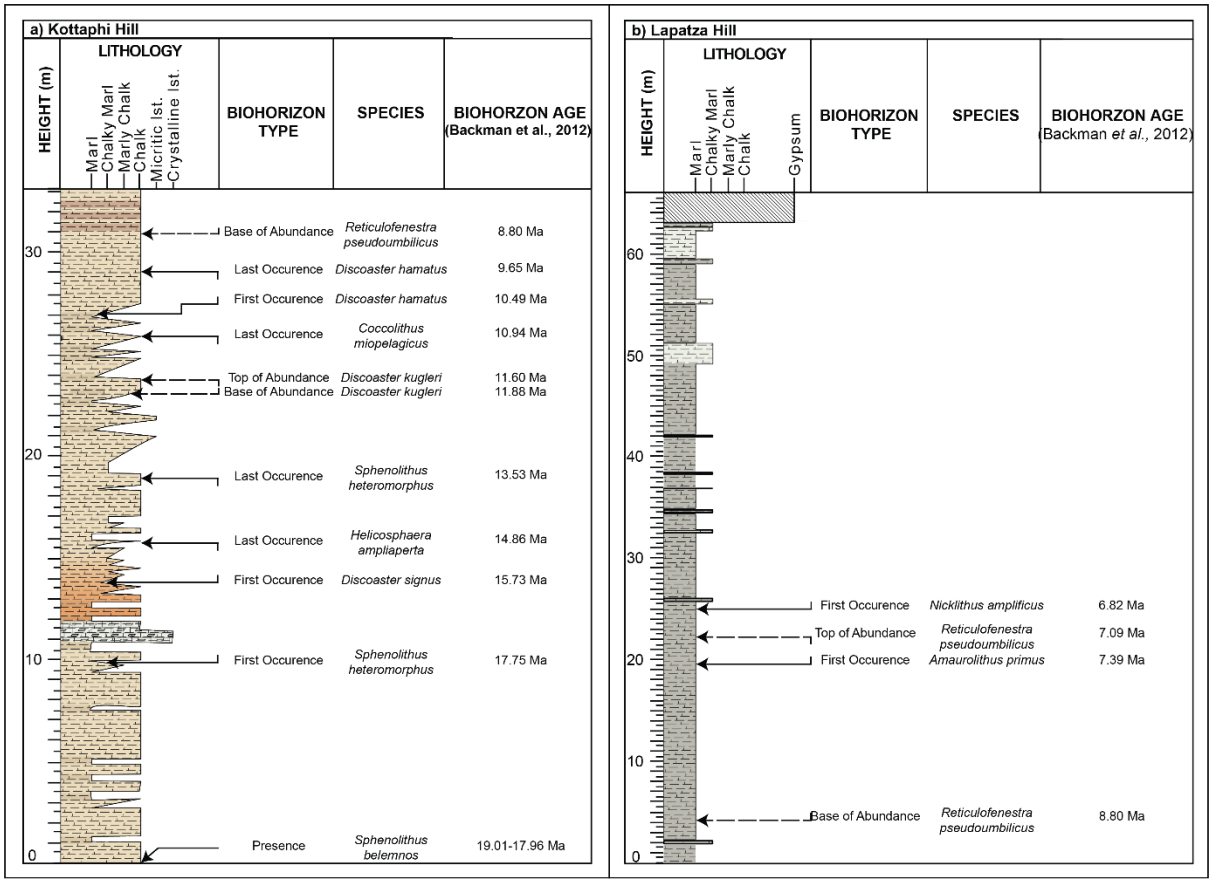

355 **Figure 4** Stratigraphic logs of the successions sampled at Kottaphi Hill (a) and Lapatza Hill (b) with height and nature of bio-horizons annotated, together with ages according to Backman et al. (2012). Bio-horizons based on relative abundance (Backman et al., 2012) are less quantitative than other bio-horizons and are marked with a dashed line.

3.3 Strontium isotope dating

3.3.1 Kottaphi Hill

360 Sr isotope dating indicates that the succession at Kottaphi Hill, above the carbonate firmground, ranges from 16.22 Ma (with an error range of 16.01 Ma to 16.46 Ma) to 7.25 Ma (with an error range of 6.86 Ma to 7.82 Ma) (Fig. 5). These Sr isotopic ages indicate that these sediments retain their depositional order, with an average sedimentation rate (nondecompacted) of 0.27 cm/ky.

https://doi.org/10.5194/egusphere-2025-442
Preprint. Discussion started: 12 February 2025

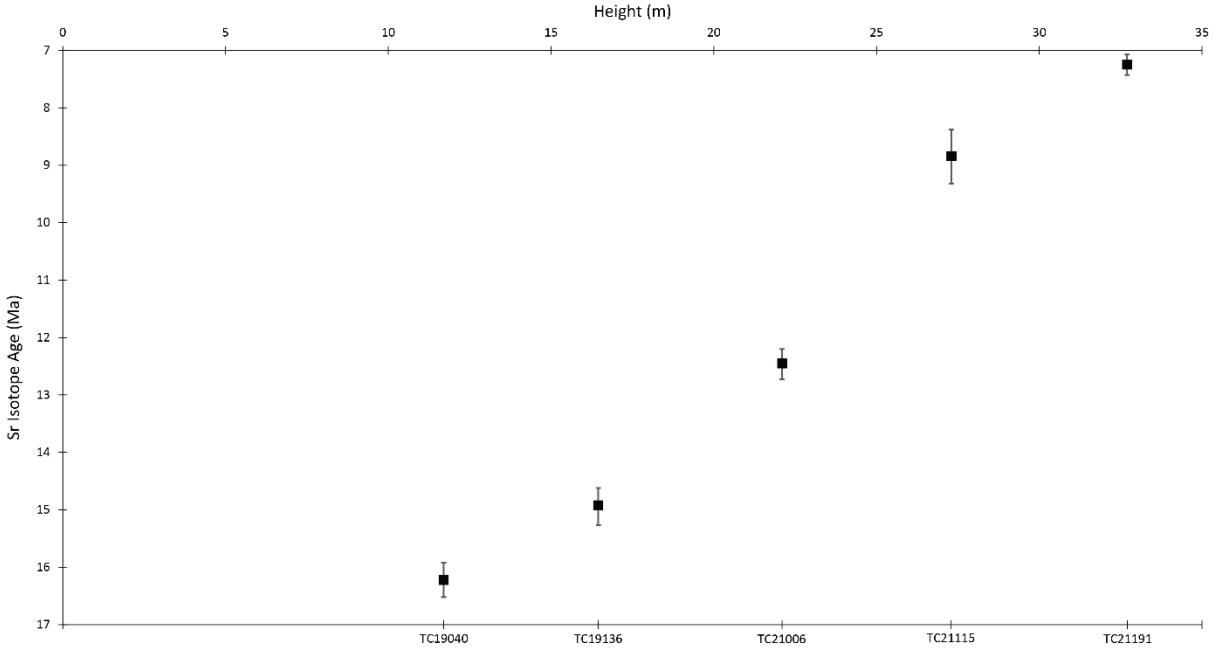

Figure 5 Sr age data for planktic foraminiferal samples from Kottaphi Hill plotted against absolute age. The determined age and the total combined error are shown for each sample.

3.3.2 Lapatza Hill

The Sr isotope data for the Lapatza Hill succession indicate an age range of 11.45 Ma (with an error range of 10.9 Ma to 12.24 Ma) to 5.44 Ma (with an error range of 5.139 Ma to 5.66 Ma) (Fig. 6). The oldest age (lowest $^{87}Sr/^{86}Sr$) is for sample TC22 330, from the 31.5 m level, whereas younger ages were calculated for the samples above and below this. Either the height of the samples up-section does not correlate with their age, or the ages determined do not represent the timing of biomineralization of these planktic foraminifer samples. There is no sedimentological or biostratigraphic evidence of the first alternative. Additionally, sample TC22 470, taken from a height of 62.75m has a strontium isotopic value (0.709241) outwith the LOWESS Sr isotope Look-Up Table (Version 4: 08/04) (McArthur *et al.*, 2001; McArthur and Howarth, 2004), indicating that this value does not represent a global seawater composition.

https://doi.org/10.5194/egusphere-2025-442
Preprint. Discussion started: 12 February 2025

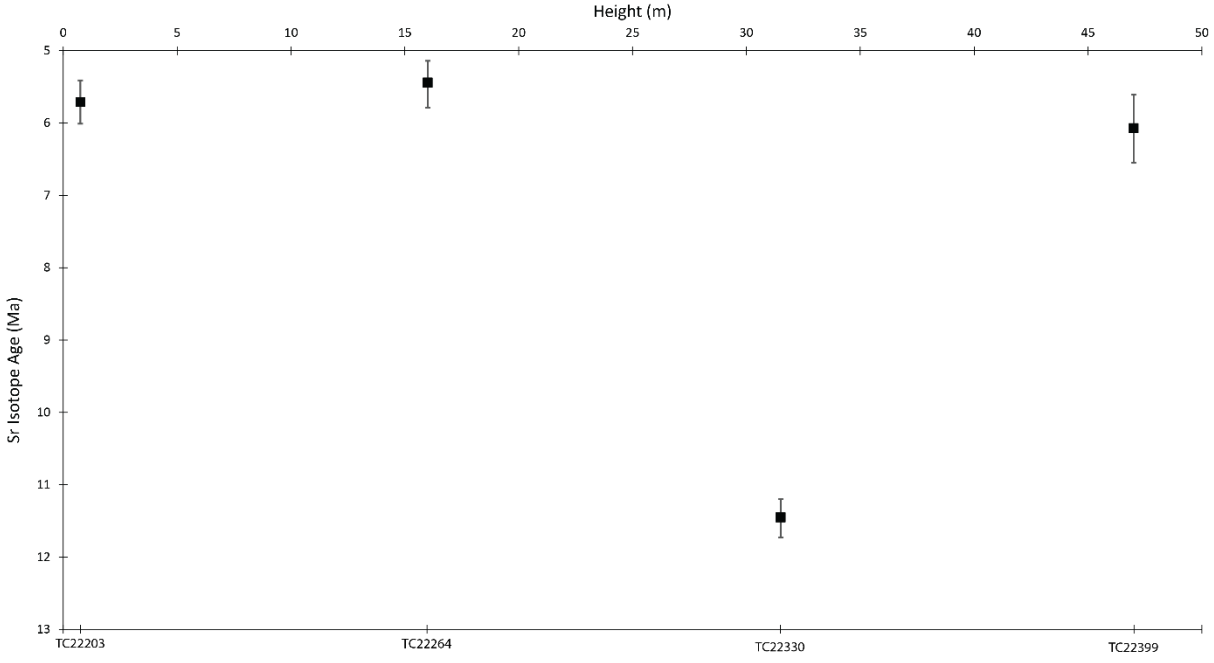

Figure 6 Sr age data for planktic foraminiferal samples from Lapatza Hill plotted against absolute age. The determined age and the total combined error are shown for each sample.

3.4 Age model

The new age model for the Kottaphi Hill indicates that the succession sampled spans 18.96 Ma (Burdigalian) to 7.72 Ma (Tortonian). From the base of the succession to 10.97 m (17.15 Ma), the average sedimentation rate was 0.805 cm/ky, whereas an average (slower) sedimentation rate of 0.245 cm/ky was calculated between 10.97 m (17.15 Ma) and the top of the succession sampled (non-decompacted)

The new age model for Lapatza Hill spans 9.14 Ma (Tortonian) to 5.74 Ma (Messinian). From the base of the succession to 25 m (6.82 Ma) the average sedimentation rate was 1.099 cm/ky, with little variation. From 25 m (6.82 Ma) to the top of the succession, sedimentation rate increased (3.627 cm/ky) (again non-decompacted).

The two sampled successions were combined to produce a composite temporal record. Figures showing the age model, together with the points used for its construction and the sedimentation rates derived from the age models for both sections are provided in the supplementary material. The composite temporal record provides indications of any changes in climatic and environmental conditions throughout the whole of the time interval of interest. A small peak (heavier $\delta^{18}O$ values) in $\delta^{18}O_{planktic}$ is noted in both records at 8.60 Ma. This point (8.60 Ma) was selected as the splice point to combine the two records to create a representative composite record, due to the similarity in $\delta^{18}O_{planktic}$, $\delta^{18}O$bulk, $\delta^{13}C_{planktic}$ and $\delta^{13}C_{bulk}$ trends and values at this point. This spliced interval provides a *c.* 13.2 My record from 18.95 Ma (Burdigalian) to 5.74 Ma (Messinian). This composite record covers the whole time interval of interest from the onset of the Miocene Climatic Optimum to the onset of the Messinian Salinity Crisis.

https://doi.org/10.5194/egusphere-2025-442
Preprint. Discussion started: 12 February 2025

3.5 Stable Isotopes

3.5.1 $\delta^{18}O$

Figure 7 shows the $\delta^{18}O_{planktic}$ and $\delta^{18}O_{finefraction}$ records for the composite temporal record and allows comparisons between the two methods. Both records show a generally similar trend for the Kottaphi Hill succession. Although the $\delta^{18}O_{planktic}$ record appears to be more variable than the $\delta^{18}O_{finefraction}$ record, both display approximately synchronous peaks and troughs. Prior to the beginning of the $\delta^{18}O_{planktic}$ record, the $\delta^{18}O_{finefraction}$ record shows a very gradual decrease in $\delta^{18}O$ (lighter $\delta^{18}O$ values). The two records show a striking divergence at the splice point, at the beginning of the Lapatza Hill succession. While the $\delta^{18}O_{planktic}$ record for Lapatza Hill continues at a similar $\delta^{18}O$ value to the Kottaphi Hill succession, the $\delta^{18}O_{finefraction}$ record exhibits a dramatic (*c.* 6.0 ‰ VDPB) offset between the two successions. The $\delta^{18}O_{finefraction}$ time series also records increased variability in $\delta^{18}O$ values for the Lapatza Hill succession compared to the Kottaphi Hill succession. The two stable isotope records (planktic and bulk sample) show different trends for the Lapatza Hill succession. However, both records show the highest (heaviest) $\delta^{18}O$ values for the Lapatza Hill succession at *c.* 6 Ma.

https://doi.org/10.5194/egusphere-2025-442
Preprint. Discussion started: 12 February 2025

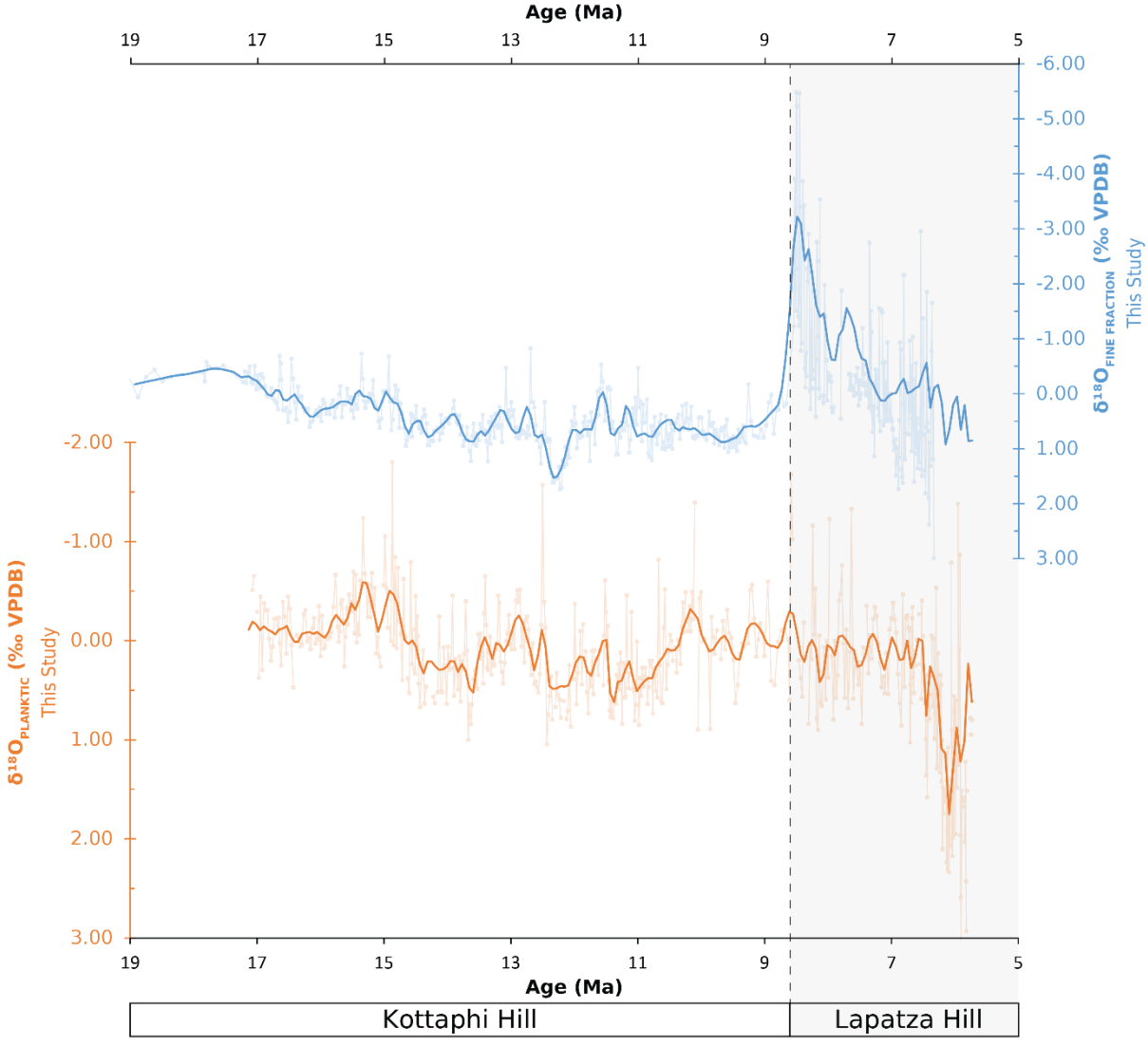

Figure 7 Plot of $\delta^{18}O_{planktic}$ (orange) and $\delta^{18}O_{finefraction}$ (blue) versus age for the composite temporal record. Measurements are shown relative to VDPB. All measured data are shown with a thin line and box markers; bold lines show the $\delta^{18}O$ data smoothed by a locally weighted function over 60 kyr (see supplementary material for additional information).

3.5.2 $\delta^{13}C$

The $\delta^{13}C$ data for the composite temporal record are shown in Fig. 8. For the Kottaphi Hill succession, the two records (planktic and bulk sample) follow a similar trend, although the $\delta^{13}C_{planktic}$ record is more variable than the $\delta^{13}C_{finefraction}$ record. The $\delta^{13}C_{planktic}$ values record a steep increase (to heavier values) in $\delta^{13}C$ at *c.* 14.6 Ma, as recorded in the $\delta^{13}C_{finefraction}$ record. Both records show a significant shift towards lighter values at the splice point between the Kottaphi Hill and Lapatza Hill records. In the $\delta^{13}C_{planktic}$ record, shortly after this shift, values return to a similar level 1-2 ‰) as in the Kottaphi Hill succession. The shift in $\delta^{13}C$ is more dramatic (*c.* 4.5 ‰) in the $\delta^{13}C_{finefraction}$ and values do not return to a similar level as in the Kottaphi Hill

https://doi.org/10.5194/egusphere-2025-442
Preprint. Discussion started: 12 February 2025

succession but instead remain lower. Following the splice point, the $\delta^{13}C_{planktic}$ and $\delta^{13}C_{finefraction}$ records show discrete trends. The $\delta^{13}C_{planktic}$ values record a second shift to lighter $\delta^{13}C$ values at *c.* 7.6 Ma, followed by a 'saw-tooth' decrease until *c.* 6.5 Ma when values sharply increased, before once again decreasing until the end of the record. In the $\delta^{13}C_{finefraction}$ record, the values continue to decrease following the negative shift at the splice point, until *c.* 8.5 Ma when values begin to increase before rapidly increasing to *c.* 0.00 ‰ at *c.* 7 Ma. $\delta^{13}C_{finefraction}$ values steadily decrease from *c.* 6.9 Ma until the end of the record.

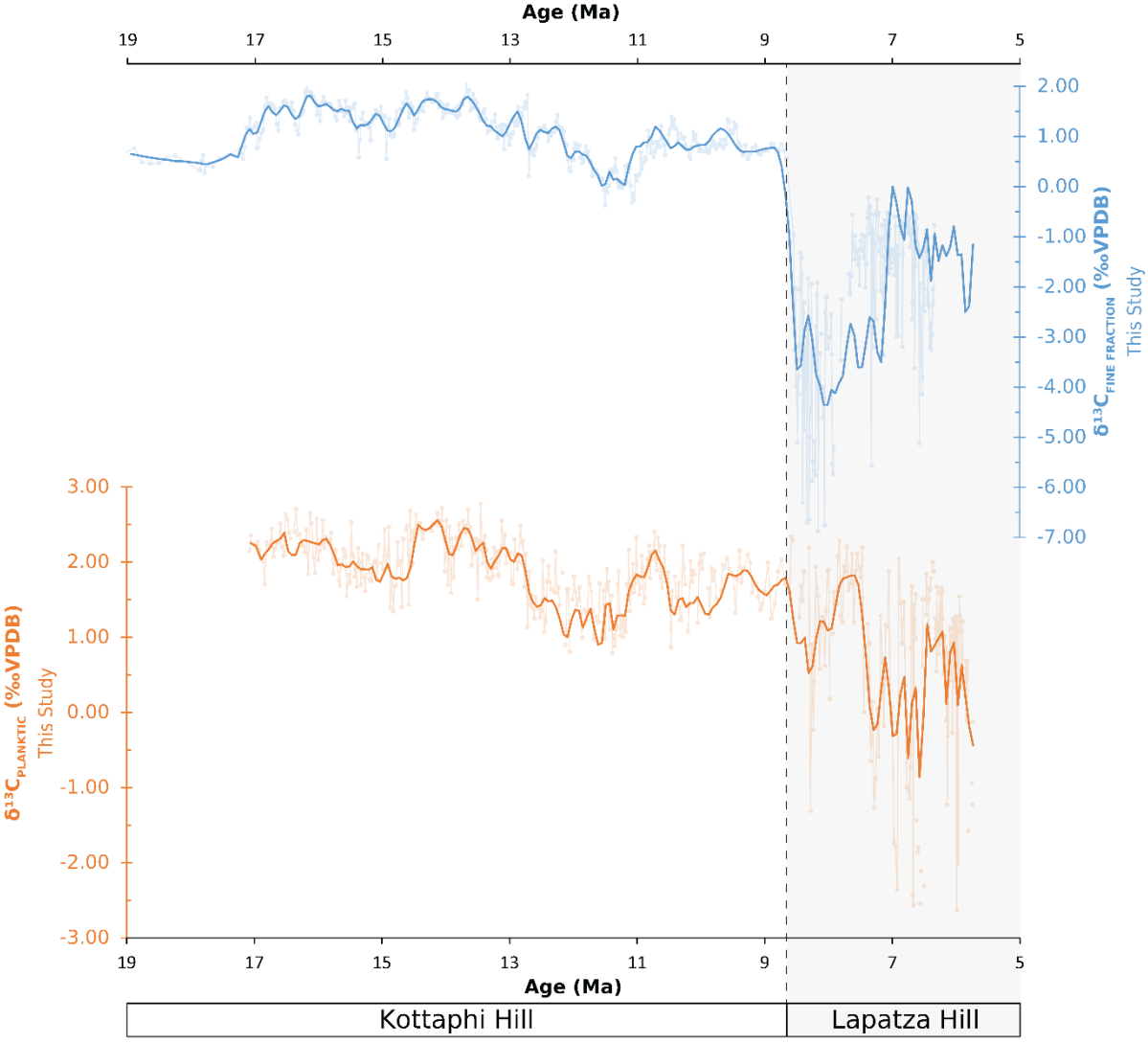

Figure 8 Plot of $\delta^{13}C_{planktic}$ (orange) and $\delta^{13}C_{finefraction}$ (blue) versus age for the composite temporal record. Measurements are shown relative to VDPB. All measured data are shown with a thin line and box markers; bold lines show these $\delta^{13}C$ data smoothed by a locally weighted function over 60 kyr (see supplementary material for additional information).

https://doi.org/10.5194/egusphere-2025-442
Preprint. Discussion started: 12 February 2025

4. Discussion

4.1 Composite Early-Late Miocene temporal record

By combining the Kottaphi Hill and Lapatza Hill data, a composite temporal record for the latest Early Miocene to the Late Miocene can be constructed (Fig. 9). As this composite temporal record combines data from the two successions sampled, the specific features of the two sections (e.g. facies; diagenesis) need to be taken into account, as detailed in Cannings (2024).

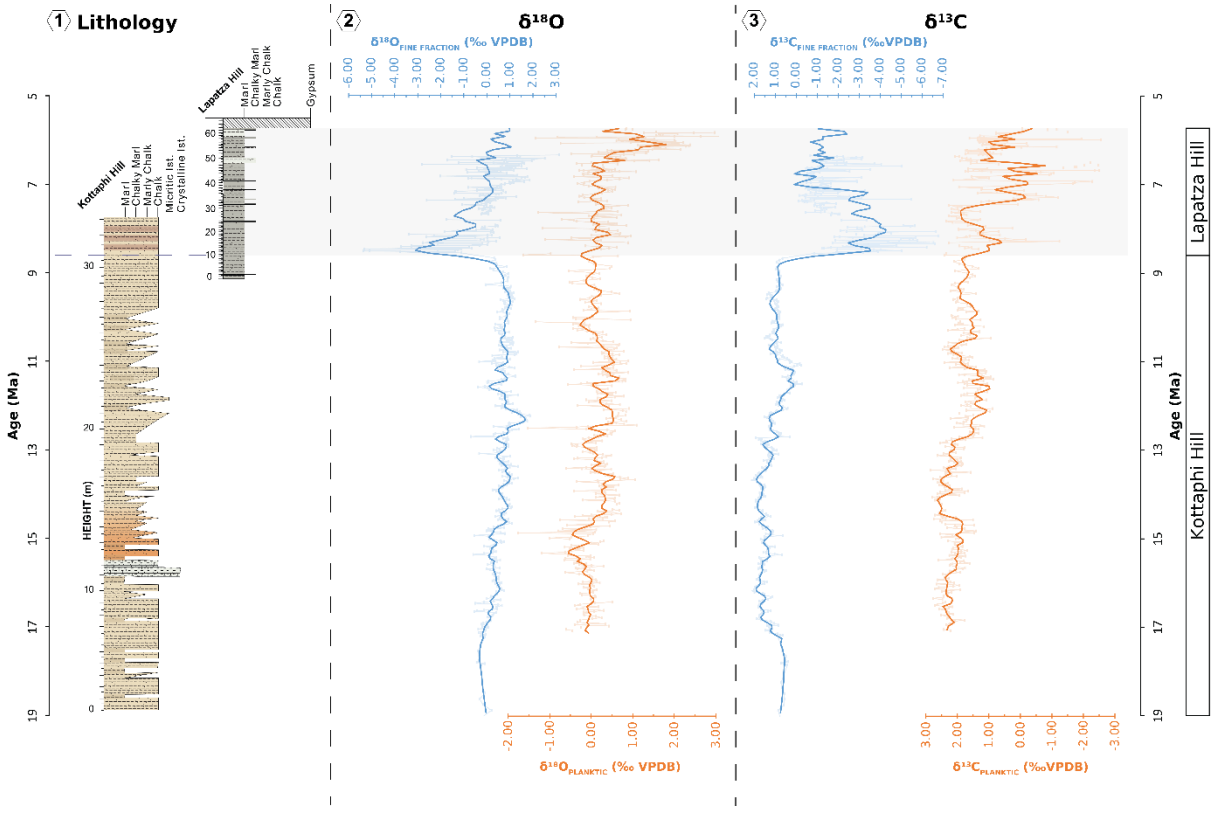

Figure 9 Stratigraphic logs of both the Kottaphi Hill succession and the Lapatza Hill succession, shown scaled to age, together with $\delta^{18}O_{planktic}$ and $\delta^{18}O_{finefraction}$ records for the composite temporal record and $\delta^{13}C_{planktic}$ and $\delta^{13}C_{finefraction}$ records for the composite temporal record. All measured or calculated data are shown with box markers connected by a thin line. Bold lines show these data smoothed by a locally weighted function over 60 kyr.

4.2 Strontium isotope dating used to support the new age model

The strontium isotope dating of the planktic foraminifera samples from Kottaphi Hill is in good agreement with the calcareous nannofossil biostratigraphic dating. The ages of the samples produced by the new age model are within the error range calculated from the Sr isotope analysis.

In contrast, the Sr isotope dating of the samples from Lapatza Hill are problematic. Sedimentological study of the succession (Cannings, 2024) did not reveal any evidence of large-scale reworking or structural overturning. Whilst diagenetic alteration is a possibility, this did not cause anomalous results in the stable isotope analyses of planktic foraminifera from Lapatza Hill.

https://doi.org/10.5194/egusphere-2025-442
Preprint. Discussion started: 12 February 2025

Anomalous $^{87}Sr/^{86}Sr$ values have been previously documented for samples of Messinian age and have been attributed to the onset of the Messinian Salinity Crisis (MSC), For example, apparently anomalous $^{87}Sr/^{86}Sr$ results have been documented from pre-evaporitic sequences in southern Turkey and attributed to variations in $^{87}Sr/^{86}Sr$ due to isolation of Mediterranean basins prior to the Messinian Salinity Crisis (Flecker and Ellam, 1999; Flecker et al., 2002; Flecker and Ellam, 2006). However, the anomalous $^{87}Sr/^{86}Sr$ values for all of the samples in this succession suggest that the onset of the MSC led to changes in the local $^{87}Sr/^{86}Sr$ of seawater c. 2 million years before the deposition of evaporites. Local changes in $^{87}Sr/^{86}Sr$ are likely to represent changes in the balance between ocean input and local changes in the hydrological cycle, as suggested based on previous modelling of $^{87}Sr/^{86}Sr$ ratios in Eastern Mediterranean basins (in SW Turkey) during the Late Miocene (Flecker et al., 2002). Modelling studies indicate that the closure of the eastern gateway of the southern Neotethys resulted in significant alterations to the hydrological cycle in the eastern Mediterranean, with evaporation exceeding freshwater input (Karami et al., 2009), which would in turn lead to variable $^{87}Sr/^{86}Sr$ values. In summary, the most likely explanation for the non-correlation of the sample height in the succession with the calculated age at Lapatza Hill is that the Sr isotope values of the planktic foraminifera analysed do not reflect the Sr isotope values of the global seawater at the time of biomineralization. Calcareous nannofossil biostratigraphy indicates that the conditions resulting in anomalous $^{87}Sr/^{86}Sr$ values were present from c. 8 Ma until the end of the recorded data during this study.

4.3 Discrepancies between stable isotope records

As noted above, the $\delta^{18}O_{finefraction}$ record (Fig. 7) shows a dramatic offset towards much lighter $\delta^{18}O$ values at the splice point between the Kottaphi Hill and Lapatza Hill successions. Similarly, the $\delta^{13}C_{finefraction}$ record shows a dramatic offset (*c.* 4.5 ‰) towards lighter $\delta^{13}C$ values at the splice point. Following this offset, both fine fraction records show different trends from the planktic records for the same sample sets from Lapatza Hill.

Interpretations based on fine fraction measurements are generally not as well constrained as those based on planktic foraminiferal measurements mainly because the former can be influenced by matrix composition. Facies observations and geochemical data indicate that the samples from the Lapatza Hill succession have a larger terrigenous component compared to those from the Kottaphi Hill succession (Cannings, 2024). The isotopic signal of the terrigenous component was therefore necessarily measured together with the biogenic carbonate signal when the fine fraction bulk samples from the Lapatza Hill succession were analyzed. Both the $\delta^{18}O_{planktic}$ and $\delta^{13}C_{planktic}$ records do not show a dramatic offset at the splice point. This supports the interpretation that the offset in the fine fraction records is due to differences in the composition of the bulk samples. A relatively low magnitude shift is noted in the $\delta^{13}C_{planktic}$ record compared to the fine fraction bulk records (Fig. 8). This shift is likely to represent small differences between the local $\delta^{13}C_{seawater}$ at each of the two localities. Localised lighter $\delta^{13}C$ values may indicate the redeposition of isotopically light carbon from a nearby shelf during sea level changes, or the input of isotopically light carbon from the continent (Vincent et al., 1980; Vincent and Berger, 1985; Kouwenhoven et al., 1999).

For the Kottaphi Hill succession, the fine fraction records are mainly influenced by the biogenic carbonate material present, as evidenced by the similarity between the fine fraction and the planktic records. As a result, the fine fraction records for Lapatza

https://doi.org/10.5194/egusphere-2025-442
Preprint. Discussion started: 12 February 2025

Hill are not suitable for interpreting climatic or oceanographic changes. The planktic record for Lapatza Hill is, however, relatively complete, limiting the need for any interpretation based on the fine fraction record. On the other hand, the fine fraction measurements of samples from Kottaphi Hill appear to be controlled by the stable isotopic composition of biogenic calcite. Therefore, the Kottaphi Hill fine fraction records can aid interpretations of climatic and oceanographic changes. This is especially useful for the interval from *c.* 19 Ma to *c.* 17 Ma when planktic foraminifera are absent or poorly preserved.

4.4 Palaeoceanographic implications4.4.1 $\delta^{18}O$

Some useful interpretations and regional to global comparisons concerning oxygen isotope trends, palaeotemperature and climatic evolution can be made based on the stable isotope records presented here (Fig. 10), in the light of the geological setting.

The trend towards lighter $\delta^{18}O_{finefraction}$ values suggests some warming in the lowermost part of the Kottaphi Hill succession between 18.96 Ma and 17.08 Ma. Relatively low $\delta^{18}O_{finefraction}$ and $\delta^{18}O_{planktic}$ values between 17.08 Ma to 14.78 Ma can be correlated to the Miocene Climatic Optimum. This period of low $\delta^{18}O$ was punctuated by three periods of inferred very high temperatures. The most prominent of these extreme periods took place at *c.* 15.7 Ma, *c.* 15.3 Ma and *c.* 14.9 Ma, consistent with an approximately 400 kyr cyclicity. Warm peaks on the *c.* 400-kyr eccentricity cycle are known from palaeotemperature records of the Pacific Ocean. These intervals are assumed to represent an ice-free Earth during the MCO, possibly the most recent ice-free periods in Earth history (Miller et al., 2005; Miller et al., 2020).

The beginning of the $\delta^{18}O$ increase recorded at *c.* 14.8 Ma correlates with Mi3a, marking the end of the MCO and the start of the MMCT (Miller et al., 1991a, b, 2020). Another positive $\delta^{18}O$ excursion at 13.8 Ma marks the Mi3 event, representing the second cooling step associated with the MMCT (Miller et al., 1991a, b,2020).

Open-ocean temperature records show slight warming and relatively stable temperatures following the first two cooling steps of the MMCT (Zachos et al., 2008; Miller et al., 2020; Westerhold et al., 2020). In contrast, the decreasing $\delta^{18}O$ that is recorded during this interval in Cyprus appears to indicate a local warming event. The cause of this apparent decoupling between global climate and eastern Mediterranean climate (using Cyprus as a reference) is uncertain but could relate to the dramatic restriction of the oceanic gateway between the Mediterranean and the Indian Ocean, which resulted in decreased interchange between the two water masses. For example, the increasingly narrow shallow water connection could have increased the volume of relatively warm seawater (heated directly by insolation and by warm river water input) to the eastern Mediterranean basin.

Following the above period of decreased $\delta^{18}O$, a positive excursion existed between 12.8 and 12.42 Ma, corresponding to the final cooling step of the MMCT and Mi4 (Miller et al., 1991b, 2020). The negative $\delta^{18}O$ excursion at *c.* 10.8 Ma was coeval with a warming event identified in a $\delta^{18}O_{benthic}$ record from the Western Pacific Ocean (Holbourn et al., 2013). This transient warming event is known as the Tortonian Thermal Maximum and is also reported in global temperature records (Westerhold et al., 2020). The warming event n the Western Pacific Ocean was transient and ended after <100kyr. However, the decreasing $\delta^{18}O$ trend recorded in the eastern Mediterranean continued until *c.* 10.2 Ma. An approximately coeval warming interval between *c.* 11 Ma and *c.* 10 Ma is noted in Mg/Ca palaeotemperature records from the Equatorial Atlantic Ocean but is not

https://doi.org/10.5194/egusphere-2025-442
Preprint. Discussion started: 12 February 2025

recorded in the Pacific Ocean (Lear et al., 2003). By this time period, temperature changes in the Southern Neotethys appear to reflect those in the Atlantic Ocean rather than the Pacific Ocean. This is consistent with limited connectivity between the Southern Neotethys and the Indian Ocean to the east by this time.

From *c.* 10.2 Ma, a long-term increasing $\delta^{18}O$ trend continued until the end of the record. This apparent cooling trend aligns with the long-term cooling trend between *c.* 10 Ma and *c.* 6 Ma, as inferred from UK_{37}' palaeotemperature records, and has been related to acceleration of Antarctic glaciation (Herbert et al., 2022). This positive $\delta^{18}O$ trend was gradual until a more dramatic increase in $\delta^{18}O$ at *c.* 6.8 Ma. This may correspond to the intense cooling from *c.* 7 Ma and *c.* 6 Ma, termed 'Late Miocene Cooling' (LMC), which is recorded in UK_{37}' palaeotemperature records for high, mid and tropical latitudes in both hemispheres of the Atlantic and Pacific oceans (Herbert et al., 2016; Tanner et al., 2020).

Following the above dramatic $\delta^{18}O$ increase, the $\delta^{18}O$ recorded measurements rapidly increased, consistent with Late Miocene warming. However, this should be taken with caution because of the extensive changes in the hydrological cycle that are attributed to the Messinian Salinity Crisis (Flecker and Ellam, 1999, 2006; Flecker *et al.*, 2002). As a result, high salinity levels are likely to have been an important control on $\delta^{18}O$ in foraminiferal calcite during this interval.

4.4.2 $\delta^{13}C$

The $\delta^{13}C_{\text{fine fraction}}$ record from Kottaphi Hill shows a period of elevated $\delta^{13}C$ values between *c.* 17 Ma and *c.* 13.5 Ma (Fig. 8). This is also recorded in the $\delta^{13}C_{\text{planktic}}$ record, albeit not as well defined (Fig. 8). This interval correlates with the well-documented Monterey global carbon isotope event (Vincent and Berger, 1985; Holbourn et al., 2007; Holbourn et al., 2015) (Fig. 10). The Monterey Event is associated with increased biological carbon isotope fractionation under high CO_2 conditions, together with enhanced burial of organic matter on continental shelves presumably as a result of eustatic sea-level rise (Sosdian et al., 2020).

Both the $\delta^{13}C_{\text{fine fraction}}$ and the $\delta^{13}C_{\text{planktic}}$ data for the composite temporal record show a gradual decrease in $\delta^{13}C$ following the Monterey Event (Fig. 10). This decrease, which is also noted in open ocean records (Cramer et al., 2009), has been related to increased CO_2 drawdown following the high CO_2 conditions of the Monterey Event (Vincent and Berger, 1985; Flower and Kennett, 1993; Flower and Kennett, 1994; Sosdian et al., 2020). Both the $\delta^{13}C_{\text{fine fraction}}$ and $\delta^{13}C_{\text{planktic}}$ are especially low at *c.* 12 Ma. This trend towards lighter $\delta^{13}C$ may also relate to reduced primary productivity in the ocean, in response to the onset of the Miocene Carbonate Crash (Holbourn et al., 2018; Holbourn et al., 2021).

The $\delta^{13}C_{\text{fine fraction}}$ and $\delta^{13}C_{\text{planktic}}$ records both show a shift to heavier values at *c.* 10.8 Ma (Fig. 10). This corresponds to the Tortonian Thermal Maximum, which is recorded at a high magnitude in the palaeotemperature records from this succession.

At 7.2 Ma, a dramatic shift (*c.* 2.5 ‰) to lighter carbon isotope values is shown in the $\delta^{13}C_{\text{planktic}}$ record (Fig. 10). This shift corresponds to the Late Miocene Carbon Isotope Shift (LMCIS) and the onset of the Late Miocene-Early Pliocene Biogenic Bloom (Dickens and Owen, 1999; Diester-Haass et al., 2004; Diester-Haass et al., 2005). Although the LMCIS is recorded in the new $\delta^{13}C_{\text{planktic}}$ record, after this time the $\delta^{13}C_{\text{planktic}}$ record does not appear to reflect the open ocean record from the North Atlantic (Cramer et al., 2009). This suggests that after *c.* 7.2 Ma (early Messinian), the $\delta^{13}C$ composition of the seawater in the

https://doi.org/10.5194/egusphere-2025-442
Preprint. Discussion started: 12 February 2025

eastern Mediterranean basins, including Cyprus, was no longer strongly influenced by global $\delta^{13}C$ changes. A change in benthic foraminiferal assemblages and a shift to lighter $\delta^{13}C$ values in the West Alboran Basin (Western Mediterranean) at 7.17 Ma has been related to the restriction of the Mediterranean-Atlantic gateway (Bulian et al., 2022). In the Lapatza Hill succession, a change in the benthic foraminiferal assemblage is noted at 7.23 Ma. Distinguishing between the effects of the LMCIS and the restriction of gateways in the west and/or the east is difficult. However, some effect of gateway closure is suggested by the discrete $\delta^{13}C$ trend recorded in the Lapatza Hill succession after *c.* 7.2 Ma. The well- documented constriction of the eastern gateway to the Indian Ocean during the Early Miocene, especially in SE Turkey (Hüsing et al., 2009; Bialik et al., 2019; Torfstein and Steinberg, 2020) is likely to have influenced the lighter carbon isotope values.

https://doi.org/10.5194/egusphere-2025-442
Preprint. Discussion started: 12 February 2025

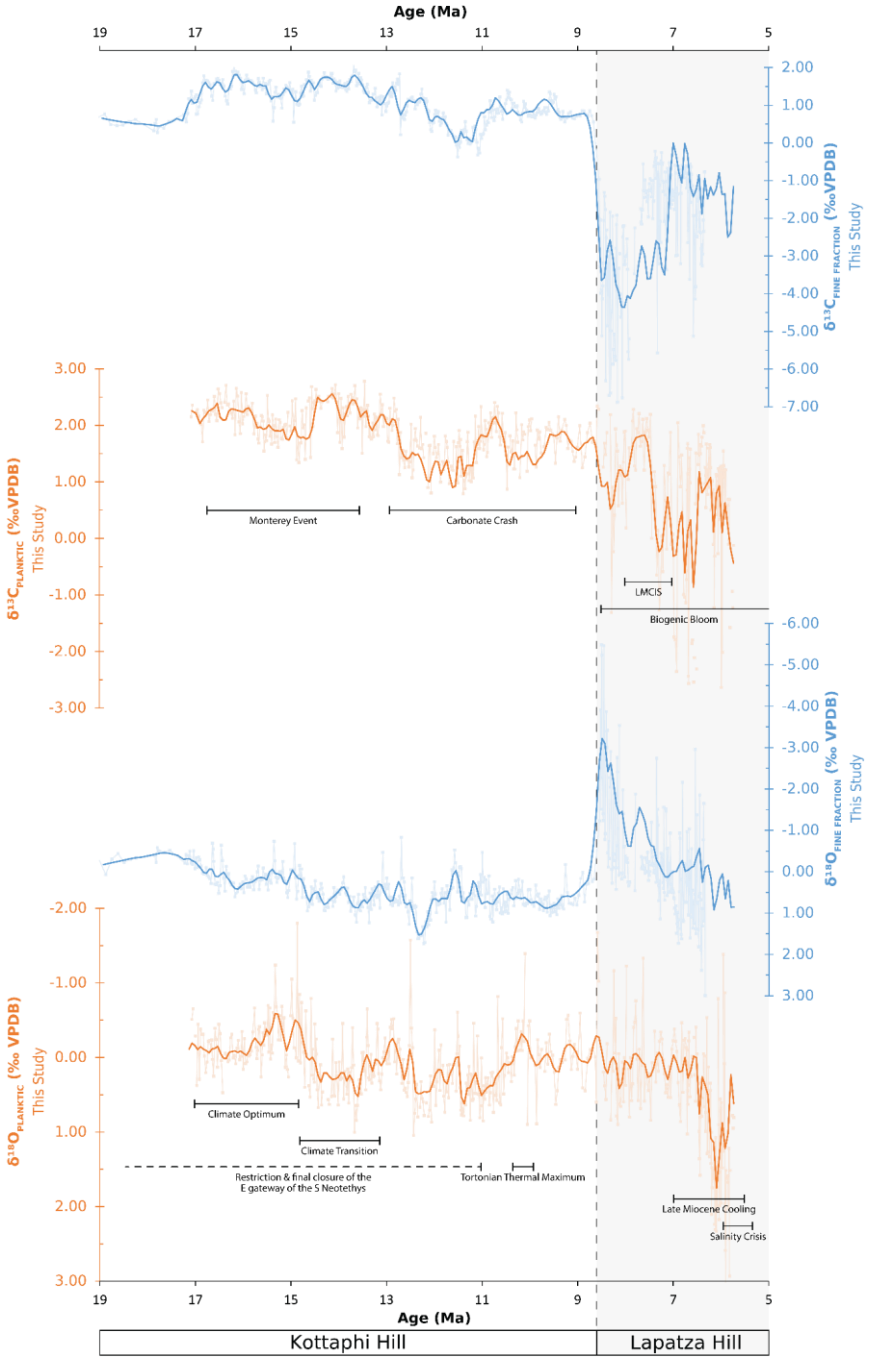

Figure 10 Plot of planktic and fine fraction δ13C and δ18O versus age for the composite temporal record. Measurements are shown relative to VDPB. Both smoothed and calculated data are shown, as in Fig. 9. The timing of several global to regional-scale oceanographic events are also indicated: (1) The Monterey Event (Vincent and Berger, 1985; Holbourn et al., 2015); (2) Miocene Carbonate Crash (Lyle et al., 1995; Lübbers et al., 2019); (3) Biogenic Bloom (Dickens and Owen, 1999; Diester-Haass et al., 2004; Diester-Haass et al., 2005); (4) Late Miocene Carbon Isotope Shift (LMCIS) (Hodell et al., 1994); (5) The Miocene Climatic Optimum (Zachos et al., 2008; Holbourn et al., 2015; Westerhold et al., 2020); (6) Restriction (from c. 20 Ma) and closure of the eastern gateway o

https://doi.org/10.5194/egusphere-2025-442
Preprint. Discussion started: 12 February 2025

f the Southern Neotethys (Hüsing et al., 2009; Bialik et al., 2019); (7) The Miocene Climate Transition (Holbourn et al., 2015; Westerhold et al., 2020); (8) The Tortonian Thermal Maximum (Westerhold et al., 2020); (9) Late Miocene Cooling (Herbert et al., 2016); (10) The Messinian Salinity Crisis (Krijgsman et al., 1999a).

4.5 Wider implications

This research provides the first-of-its-kind long-term $\delta^{13}C$ and $\delta^{18}O$ stable isotope record for the eastern Mediterranean region. This new record provides a useful reference section for future studies of Miocene eastern Mediterranean palaeoceanography. Whilst the trends recorded for global events such as the MMCO, MMCT and the Monterey event were anticipated, this new record reveals an extreme and long-lasting oxygen isotope excursion coinciding with the Tortonion Thermal Maximum. The apparent discrepancy in magnitude between this event in Cyprus and the event recorded in global records warrants further examination. It is possible that the discrepancy may related to the developing restriction in connectivity of the eastern Mediterranean Sea and the open ocean. Further research to distinguish the $\delta^{13}C$ signal related to the LCMIS from regional $\delta^{13}C$ trends related to the restriction and closure of ocean gateways would also be a useful extension of this study.

5 Conclusions

- A shift in $\delta^{13}C$ and $\delta^{18}O$ fine fraction values between two successions studied in Cyprus, the Kottaphi Hill succession and the Lapatza Hill succession, is explained by a larger terrigenous component in samples from the Lapatza Hill succession. Although fine-fraction samples can be used effectively for sites with a low terrigenous input (such as Kottaphi Hill), care must be taken to avoid recording signals unrelated to biogenic carbonate material where background terrigenous input is high.
- The Early-Middle Miocene Monterey Event is clearly recorded in the composite temporal $\delta^{13}C$ record that was produced by splicing of the two correlative successions (Lapatza and Kottaphi Hill).
- The new composite $\delta^{18}O$ record from Cyprus allows the recognition of global climate events such as the Miocene Climatic Optimum, the Middle Miocene Climate Transition and the Late Miocene Cooling. The decreasing $\delta^{18}O$ trend at the Tortonian Thermal Maximum appears to have continued for longer in the eastern Mediterranean (using Cyprus as a reference) than in global records. This may represent a local to regional-scale warming event, during a time when there was apparently extensive variation and disequilibrium, both between and within the Atlantic and Pacific oceans.
- A negative shift in $\delta^{13}C_{planktic}$ values at *c.* 7.2 Ma may correlate with the global 'Late Miocene Carbon Isotope Shift'. However, it is difficult to distinguish the effects of the LMCIS from regional $\delta^{13}C$ trends due to the partial closure of the gateways, both between the Mediterranean Sea-Atlantic Ocean and between the Mediterranean sea and the Indian Ocean.
- This new composite stable isotope record from Cyprus provides a useful reference section for the study of oceanographic changes in the eastern Mediterranean basins during the Miocene, in relation to the western Mediterranean basins and elsewhere.

https://doi.org/10.5194/egusphere-2025-442
Preprint. Discussion started: 12 February 2025

Author Contribution

TC, AHFR and DK designed the research and carried out the initial fieldwork together. TC carried out the nannofossil dating and analysis. TC, AHFR, and DK discussed and interpreted the resulting data. TC produced the figures. TC and AHFR wrote the manuscript.

Competing Interests

The authors declare that they have no conflict of interest.

Acknowledgements

This paper is based on studies carried out for the PhD degree by T.C. at the University of Edinburgh. This research was funded by a Natural Environment Research Council E^4 DTP studentship (NE/S007407/1). We thank E. de Leau for her help and support with this research. We are also grateful to S. Jung for his help with the production of the age model. We thank C. Chilcott and U. Baranowski for their assistance with stable isotope analysis. We also thank A. Kelly and V. Gallagher, Scottish Universities Environmental Research Centre, East Kilbride, for their assistance with the Sr isotopic analysis. T.C. thanks E. Balmer and J. Shearer for their help during fieldwork, and also I. Raffi for her guidance and training in calcareous nannofossil biostratigraphy.

References

Adams, C. G., Benson, R. H., Kidd, R. B., Ryan, W. B. F., and Wright, R. C.: The Messinian salinity crisis and evidence of late Miocene eustatic changes in the world ocean, Nature, 269, 10.1038/269383a0, 1977.

Anderson, T. F. and Cole, S. A.: The stable isotope geochemistry of marine coccoliths; a preliminary comparison with planktonic foraminifera, Journal of Foraminiferal Research, 5, 188-192, 10.2113/GSJFR.5.3.188, 1975.

Artiaga, D., García-Veigas, J., Cendón, D. I., Atalar, C., and Gibert, L.: The Messinian evaporites of the Mesaoria basin (North Cyprus): A discrepancy with the current chronostratigraphic understanding, Palaeogeography, Palaeoclimatology, Palaeoecology, 584, 110681-110681, https://doi.org/10.1016/j.palaeo.2021.110681, 2021.

Athanasiou, M., Triantaphyllou, M. V., Dimiza, M. D., Gogou, A., Panagiotopoulos, I., Arabas, A., Skampa, E., Kouli, K., Hatzaki, M., and Tsiolakis, E.: Reconstruction of oceanographic and environmental conditions in the eastern Mediterranean (Kottafi Hill section, Cyprus Island) during the middle Miocene Climate Transition, Revue de Micropaléontologie, 70, 100480-100480, 10.1016/J.REVMIC.2020.100480, 2021.

Aze, T., Ezard, T. H. G., Purvis, A., Coxall, H. K., Stewart, D. R. M., Wade, B. S., and Pearson, P. N.: A phylogeny of Cenozoic macroperforate planktonic foraminifera from fossil data, Biological Reviews, 86, 900-927, 10.1111/J.1469-185X.2011.00178.X, 2011.

https://doi.org/10.5194/egusphere-2025-442
Preprint. Discussion started: 12 February 2025

Backman, J. and Shackleton, N. J.: Quantitative biochronology of Pliocene and early Pleistocene calcareous nannofossils from the Atlantic, Indian and Pacific oceans, Marine Micropaleontology, 8, 141-170, 10.1016/0377-8398(83)90009-9, 1983.

Backman, J., Raffi, I., Rio, D., Fornaciari, E., and Pälike, H.: Biozonation and biochronology of miocene through pleistocene calcareous nannofossils from low and middle latitudes, Newsletters on Stratigraphy, 45, 221-244, 10.1127/0078-0421/2012/0022, 2012.

Bagnall, P. S.: The geology and mineral resources of the Pano Lefkara-Larnaca area, authority of the Government of Cyprus, 1960.

Balmer, E. M.: Interaction of deep and shallow-water sedimentary processes in southwest Cyprus, within the Eastern Mediterranean region., University of Edinburgh, Unpublished PhD Thesis, 2024.

Bialik, O. M., Frank, M., Betzler, C., Zammit, R., and Waldmann, N. D.: Two-step closure of the Miocene Indian Ocean Gateway to the Mediterranean, Scientific Reports, 9, 8842-8842, 10.1038/s41598-019-45308-7, 2019.

Blow, W. H.: Origin and Evolution of the Foraminiferal Genus Orbulina d'Orbigny, Micropaleontology, 2, 57-57, 10.2307/1484492, 1956.

Bown, P. R. and Young, J. R.: Techniques in: Calcareous Nannofossil Biostratigraphy, Paleoceanography, 1998.

Bulian, F., Kouwenhoven, T. J., Jiménez-Espejo, F. J., Krijgsman, W., Andersen, N., and Sierro, F. J.: Impact of the Mediterranean-Atlantic connectivity and the late Miocene carbon shift on deep-sea communities in the Western Alboran Basin, Palaeogeography, Palaeoclimatology, Palaeoecology, 589, 110841-110841, https://doi.org/10.1016/j.palaeo.2022.110841, 2022.

Cannings, T.: Middle-Late Miocene palaeoceanographic development of Cyprus (E. Mediterranean) based on integrated study of $\delta^{18}O$ and $\delta^{13}C$ stable isotope records, supported by Mg/Ca palaeothermometry, nannofossil biostratigraphy, Sr isotopic dating, sedimentology and other geochemical data, School of Geosciences, University of Edinburgh, Edinburgh, 412 pp., 10.7488/era/4125, 2024.

Cannings, T., Balmer, E. M., Coletti, G., Ickert, R. B., Kroon, D., Raffi, I., and Robertson, A. H. F.: Microfossil and strontium isotope chronology used to identify the controls of Miocene reefs and related facies in NW Cyprus, Journal of the Geological Society, 178, 10.1144/jgs2020-081, 2021.

Chen, G., Robertson, A. H. F., and Wu, F. Y.: Detrital zircon geochronology and related evidence from clastic sediments in the Kyrenia Range, N Cyprus: Implications for the Mesozoic-Cenozoic erosional history and tectonics of southern Anatolia, Earth-Science Reviews, 233, 10.1016/J.EARSCIREV.2022.104167, 2022.

Coletti, G., Balmer, E. M., Bialik, O. M., Cannings, T., Kroon, D., Robertson, A. H. F., and Basso, D.: Microfacies evidence for the evolution of Miocene coral-reef environments in Cyprus, Palaeogeography, Palaeoclimatology, Palaeoecology, 584, 10.1016/j.palaeo.2021.110670, 2021.

Cramer, B. S., Toggweiler, J. R., Wright, J. D., Katz, M. E., and Miller, K. G.: Ocean overturning since the late cretaceous: Inferences from a new benthic foraminiferal isotope compilation, Paleoceanography, 24, 10.1029/2008PA001683, 2009.

Darin, M. H. and Umhoefer, P. J.: Diachronous initiation of Arabia-Eurasia collision from eastern Anatolia to the southeastern Zagros Mountains since middle Eocene time, International Geology Review, 64, 2653-2681, 10.1080/00206814.2022.2048272, 2022.

https://doi.org/10.5194/egusphere-2025-442
Preprint. Discussion started: 12 February 2025

Davies, Q. J.: Climatic and tectonic controls on deep water sedimentary cyclicity: evidence from the Miocene to Pleistocene of Cyprus, Open University (United Kingdom)2001.

De Vleeschouwer, D., Vahlenkamp, M., Crucifix, M., and Pälike, H.: Alternating Southern and Northern Hemisphere climate response to astronomical forcing during the past 35 m.y, Geology, 45, 375-378, 10.1130/G38663.1, 2017.

Dickens, G. R. and Owen, R. M.: The Latest Miocene-Early Pliocene biogenic bloom: A revised Indian Ocean perspective, Marine Geology, 10.1016/S0025-3227(99)00057-2,

Diester-Haass, L., Billups, K., and Emeis, K. C.: In search of the late Miocene-early Pliocene "biogenic bloom" in the Atlantic Ocean (Ocean Drilling Program Sites 982, 925, and 1088), Paleoceanography, 20, 10.1029/2005PA001139, 2005.

Diester-Haass, L., Meyers, P. A., and Bickert, T.: Carbonate crash and biogenic bloom in the late Miocene: Evidence from ODP Sites 1085, 1086, and 1087 in the Cape Basin, southeast Atlantic Ocean, Paleoceanography, 19, 10.1029/2003PA000933, 2004.

Eaton, S. and Robertson, A. H. F.: The Miocene Pakhna Formation, southern Cyprus and its relationship to the Neogene tectonic evolution of the Eastern Mediterranean, Sedimentary Geology, 86, 10.1016/0037-0738(93)90026-2, 1993.

Elderfield, H.: Strontium isotope stratigraphy, Palaeogeography, Palaeoclimatology, Palaeoecology, 57, 71-90, 10.1016/0031-0182(86)90007-6, 1986.

Flecker, R. and Ellam, R. M.: Distinguishing climatic and tectonic signals in the sedimentary successions of marginal basins using Sr isotopes: An example from the Messinian salinity crisis, Eastern Mediterranean, Journal of the Geological Society, 156, 847-854, 10.1144/GSJGS.156.4.0847, 1999.

Flecker, R. and Ellam, R. M.: Identifying Late Miocene episodes of connection and isolation in the Mediterranean–Paratethyan realm using Sr isotopes, Sedimentary Geology, 188-189, 189-203, 10.1016/J.SEDGEO.2006.03.005, 2006.

Flecker, R., De Villiers, S., and Ellam, R. M.: Modelling the effect of evaporation on the salinity-87Sr/86Sr relationship in modern and ancient marginal-marine systems: The Mediterranean Messinian Salinity Crisis, Earth and Planetary Science Letters, 203, 221-233, 10.1016/S0012-821X(02)00848-8, 2002.

Flecker, R., Krijgsman, W., Capella, W., de Castro Martíns, C., Dmitrieva, E., Mayser, J. P., Marzocchi, A., Modestu, S., Ochoa, D., Simon, D., Tulbure, M., van den Berg, B., van der Schee, M., de Lange, G., Ellam, R., Govers, R., Gutjahr, M., Hilgen, F., Kouwenhoven, T., Lofi, J., Meijer, P., Sierro, F. J., Bachiri, N., Barhoun, N., Alami, A. C., Chacon, B., Flores, J. A., Gregory, J., Howard, J., Lunt, D., Ochoa, M., Pancost, R., Vincent, S., and Yousfi, M. Z.: Evolution of the Late Miocene Mediterranean–Atlantic gateways and their impact on regional and global environmental change, Earth-Science Reviews, 150, 365-392, 10.1016/J.EARSCIREV.2015.08.007, 2015.

Flower, B. P. and Kennett, J. P.: Middle Miocene ocean-climate transition: High-resolution oxygen and carbon isotopic records from Deep Sea Drilling Project Site 588A, southwest Pacific, Paleoceanography, 8, 811-843, 10.1029/93PA02196, 1993.

Flower, B. P. and Kennett, J. P.: The middle Miocene climatic transition: East Antarctic ice sheet development, deep ocean circulation and global carbon cycling, Palaeogeography, Palaeoclimatology, Palaeoecology, 108, 537-555, 10.1016/0031-0182(94)90251-8, 1994.

Follows, E. J.: Sedimentology and tectonic setting of Miocene reef and related sediments in Cyprus, 1990.

https://doi.org/10.5194/egusphere-2025-442
Preprint. Discussion started: 12 February 2025

Follows, E. J.: Patterns of reef sedimentation and diagenesis in the Miocene of Cyprus, Sedimentary Geology, 79, 10.1016/0037-0738(92)90013-H, 1992.

Follows, E. J. and Robertson, A. H. F.: Sedimentology and structural setting of Miocene reefal limestones in Cyprus, Troodos 1987. Symposium, 207-215,

Follows, E. J., Robertson, A. H. F., and Scoffin, T. P.: Tectonic controls on Miocene reefs and related carbonate facies in Cyprus, Models for carbonate stratigraphy from Miocene reef complexes of Mediterranean regions, 295-315, 10.2110/csp.96.01.0295, 1996.

Foster, G. L., Lear, C. H., and Rae, J. W. B.: The evolution of pCO2, ice volume and climate during the middle Miocene, Earth and Planetary Science Letters, 341-344, 243-254, https://doi.org/10.1016/j.epsl.2012.06.007, 2012.

Garcés, M., Krijgsman, W., and Agustí, J.: Chronology of the late Turolian deposits of the Fortuna basin (SE Spain): implications for the Messinian evolution of the eastern Betics, Earth and Planetary Science Letters, 163, 69-81, 10.1016/S0012-821X(98)00176-9, 1998.

Gass, I. G. and Masson-Smith, D.: The geology and gravity anomalies of the Troodos Massif, Cyprus, Philosophical Transactions of the Royal Society of London. Series A, Mathematical and Physical Sciences, 255, 417-467, 1963.

Hakyemez, Y., Turhan, N., Sonmez, I., and Sumengen, M.: Kuzey Kıbrıs Turk Cumhuriyeti'nin Jeolojisi [Geology of the Turkish Republic of Northern Cyprus], Unpublished report of MTA (Maden Tektik ve Arama), Genel Mudurlugu Jeoloji Etutleri Diaresi, Ankara, 2000.

Harzhauser, M., Kroh, A., Mandic, O., Piller, W. E., Göhlich, U., Reuter, M., and Berning, B.: Biogeographic responses to geodynamics:: A key study all around the Oligo-Miocene Tethyan Seaway, Zool Anz, 246, 241-256, 10.1016/j.jcz.2007.05.001, 2007.

Herbert, T. D., Dalton, C. A., Liu, Z., Salazar, A., Si, W., and Wilson, D. S.: Tectonic degassing drove global temperature trends since 20 Ma, Science, 377, 10.1126/science.abl4353, 2022.

Herbert, T. D., Lawrence, K. T., Tzanova, A., Peterson, L. C., Caballero-Gill, R., and Kelly, C. S.: Late Miocene global cooling and the rise of modern ecosystems, Nature Geoscience, 9, 843-847, 10.1038/ngeo2813, 2016.

Hodell, D. A., Benson, R. H., Kent, D. V., Boersma, A., and Rakic-El Bied, K.: Magnetostratigraphic, biostratigraphic, and stable isotope stratigraphy of an Upper Miocene drill core from the Salé Briqueterie (northwestern Morocco): A high-resolution chronology for the Messinian stage, Paleoceanography, 9, 835-855, https://doi.org/10.1029/94PA01838, 1994.

Holbourn, A., Kuhnt, W., Clemens, S. C., and Heslop, D.: A ~12 Myr Miocene Record of East Asian Monsoon Variability From the South China Sea, Paleoceanography and Paleoclimatology, 36, 10.1029/2021PA004267, 2021.

Holbourn, A., Kuhnt, W., Schulz, M., and Erlenkeuser, H.: Impacts of orbital forcing and atmospheric carbon dioxide on Miocene ice-sheet expansion, Nature, 438, 10.1038/nature04123, 2005.

Holbourn, A., Kuhnt, W., Clemens, S., Prell, W., and Andersen, N.: Middle to late Miocene stepwise climate cooling: Evidence from a high-resolution deep water isotope curve spanning 8 million years, Paleoceanography, 28, 10.1002/2013PA002538, 2013.

Holbourn, A., Kuhnt, W., Kochhann, K. G. D., Andersen, N., and Sebastian Meier, K. J.: Global perturbation of the carbon cycle at the onset of the Miocene Climatic Optimum, Geology, 43, 123-126, 10.1130/G36317.1, 2015.

https://doi.org/10.5194/egusphere-2025-442
Preprint. Discussion started: 12 February 2025

Holbourn, A., Kuhnt, W., Kochhann, K. G. D., Matsuzaki, K. M., and Andersen, N.: Middle Miocene climate–carbon cycle dynamics: Keys for understanding future trends on a warmer Earth?, Understanding the Monterey Formation and Similar Biosiliceous Units across Space and Time, 10.1130/2022.2556(05), 2022.

Holbourn, A., Kuhnt, W., Schulz, M., Flores, J.-A., and Andersen, N.: Orbitally-paced climate evolution during the middle Miocene "Monterey" carbon-isotope excursion, Earth and Planetary Science Letters, 261, 534-550, https://doi.org/10.1016/j.epsl.2007.07.026, 2007.

Holbourn, A. E., Kuhnt, W., Clemens, S. C., Kochhann, K. G. D., Jöhnck, J., Lübbers, J., and Andersen, N.: Late Miocene climate cooling and intensification of southeast Asian winter monsoon, Nature Communications, 9, 10.1038/s41467-018-03950-1, 2018.

Hsü, K. J.: The messinian salinity crisis - Evidence of Late Miocene eustatic changes in the world ocean, Naturwissenschaften, 65, 10.1007/BF00440344, 1978.

Hsü, K. J., Cita, M. B., and Ryan, W. B. F.: 43 . The origin of the Mediterranean evaporites, Init. Rep. DSDP, XIII, 1973a.

Hsü, K. J., Ryan, W. B. F., and Cita, M. B.: Late miocene desiccation of the mediterranean, Nature, 242, 240-244, 10.1038/242240a0, 1973b.

Hüsing, S. K., Zachariasse, W. J., Van Hinsbergen, D. J. J., Krijgsman, W., Inceöz, M., Harzhauser, M., Mandic, O., and Kroh, A.: Oligocene-miocene basin evolution in se anatolia, turkey: Constraints on the closure of the eastern tethys gateway, Geological Society Special Publication, 311, 107-132, 10.1144/SP311.4, 2009.

Jacobs, E., Weissert, H., Shields, G., and Stille, P.: The Monterey event in the Mediterranean: A record from shelf sediments of Malta, Paleoceanography, 11, 10.1029/96PA02230, 1996.

Kähler, G. and Stow, D. A. V.: Turbidites and contourites of the Palaeogene Lefkara Formation, southern Cyprus, Sedimentary Geology, 115, 215-231, 10.1016/S0037-0738(97)00094-8, 1998.

Kasbohm, J. and Schoene, B.: Rapid eruption of the Columbia River flood basalt and correlation with the mid-Miocene climate optimum, Science Advances, 4, eaat8223-eaat8223, 10.1126/sciadv.aat8223, 2018.

Kennett, J. P., Houtz, R. E., and Shackleton, N. J.: Paleotemperature History of the Cenozoic and the Initiation of Antarctic Glaciation: Oxygen and Carbon Isotope Analyses in DSDP Sites 277, 279 and 281, in: Initial Reports of the Deep Sea Drilling Project, 29, U. S. Government Printing Office, 743-756, 10.2973/dsdp.proc.29.117.1975, 1975.

Kennett, J. P., Exon, N. F., Kennett, J. P., and Exon, N. F.: Paleoceanographic evolution of the Tasmanian Seaway and its climatic implications, GMS, 151, 345-367, 10.1029/151GM19, 2004.

Kinnaird, T. C., Robertson, A. H. F., and Morris, A.: Timing of uplift of the Troodos Massif (Cyprus) constrained by sedimentary and magnetic polarity evidence, Journal of the Geological Society, 168, 10.1144/0016-76492009-150, 2011.

Kocsis, L., Vennemann, T. W., Fontignie, D., Baumgartner, C., Montanari, A., and Jelen, B.: Oceanographic and climatic evolution of the Miocene Mediterranean deduced from Nd, Sr, C, and O isotope compositions of marine fossils and sediments, Paleoceanography, 23, Artn Pa4211

10.1029/2007pa001540, 2008.

https://doi.org/10.5194/egusphere-2025-442
Preprint. Discussion started: 12 February 2025

Kouwenhoven, T. J., Seidenkrantz, M. S., and Van Der Zwaan, G. J.: Deep-water changes: The near-synchronous disappearance of a group of benthic foraminifera from the Late Miocene Mediterranean, Palaeogeography, Palaeoclimatology, Palaeoecology, 152, 10.1016/S0031-0182(99)00065-6, 1999.

Krijgsman, W., Hilgen, F. J., Raffi, I., Sierro, F. J., and Wilson, D. S.: Chronology, causes and progression of the Messinian salinity crisis, Nature, 400, 652-655, 10.1038/23231, 1999a.

Krijgsman, W., Blanc-Valleron, M. M., Flecker, R., Hilgen, F. J., Kouwenhoven, T. J., Merle, D., Orszag-Sperber, F., and Rouchy, J. M.: The onset of the Messinian salinity crisis in the Eastern Mediterranean (Pissouri Basin, Cyprus), Earth and Planetary Science Letters, 194, 299-310, https://doi.org/10.1016/S0012-821X(01)00574-X, 2002.

Krijgsman, W., Langereis, C. G., Zachariasse, W. J., Boccaletti, M., Moratti, G., Gelati, R., Iaccarino, S., Papani, G., and Villa, G.: Late Neogene evolution of the Taza–Guercif Basin (Rifian Corridor, Morocco) and implications for the Messinian salinity crisis, Marine Geology, 153, 147-160, 10.1016/S0025-3227(98)00084-X, 1999b.

Lapierre, H.: Les formations sédimentaires et éruptives des nappes de Mamonia et leurs rélations avec le massif de Troodos (Chypre), 1972.

Lear, C. H., Rosenthal, Y., and Wright, J. D.: The closing of a seaway: Ocean water masses and global climate change, Earth and Planetary Science Letters, 210, 10.1016/S0012-821X(03)00164-X, 2003.

Lord, A. R., Panayides, I., Urquhart, E., Xenophontos, C., and Malpas, J.: A biochronostratigraphical framework for the Late Cretaceous–Recent circum-Troodos sedimentary sequence, Cyprus, Proceedings of the Third International Conference on the Geology of the Eastern Mediterranean. Geological Survey Department, Nicosia, 297-297,

Lübbers, J., Kuhnt, W., Holbourn, A. E., Bolton, C. T., Gray, E., Usui, Y., Kochhann, K. G. D., Beil, S., and Andersen, N.: The Middle to Late Miocene "Carbonate Crash" in the Equatorial Indian Ocean, Paleoceanography and Paleoclimatology, 34, 10.1029/2018PA003482, 2019.

Lyle, M., Dadey, K. A., and Farrell, J. W.: 42. The Late Miocene (11–8 Ma) Eastern Pacific Carbonate Crash: evidence for reorganization of deep-water Circulation by the closure of the Panama Gateway, Proceedings of the ocean Drilling Program, Scientific Results, 138, 1995.

Lyle, M., Joy Drury, A., Tian, J., Wilkens, R., and Westerhold, T.: Late miocene to holocene high-resolution eastern equatorial pacific carbonate records: Stratigraphy linked by dissolution and paleoproductivity, Climate of the Past, 15, 10.5194/cp-15-1715-2019, 2019.

Mantis, M.: Upper Cretaceous-Tertiary foraminiferal zones in Cyprus, Sci. Res. Cent. of Cyprus, Epetiris, 3, 227-241, 1970.

Mantis, M.: Some Planktonic Foraminifera from South Cyprus, 1972.

Manzi, V., Lugli, S., Roveri, M., Dela Pierre, F., Gennari, R., Lozar, F., Natalicchio, M., Schreiber, B. C., Taviani, M., and Turco, E.: The Messinian salinity crisis in Cyprus: a further step towards a new stratigraphic framework for Eastern Mediterranean, Basin Research, 28, 207-236, 10.1111/bre.12107, 2016.

McArthur, J. M. and Howarth, R. J.: Sr-isotope stratigraphy, in: Geological Timescale 2004, edited by: Gradstein, F. M., Ogg, J. G., and Smith, A. G., Cambridge University Press, Cambridge, 589-589, 2004.

https://doi.org/10.5194/egusphere-2025-442
Preprint. Discussion started: 12 February 2025

McArthur, J. M., Howarth, R. J., and Bailey, T. R.: Strontium isotope stratigraphy: LOWESS version 3: Best fit to the marine Sr-isotope curve for 0-509 Ma and accompanying look-up table for deriving numerical age, Journal of Geology, 109, 155-170, 10.1086/319243/ASSET/IMAGES/LARGE/FG9.JPEG, 2001.

McCay, G. A., Robertson, A. H. F., Kroon, D., Raffi, I., Ellam, R. M., and Necdet, M.: Stratigraphy of Cretaceous to Lower Pliocene sediments in the northern part of Cyprus based on comparative 87Sr/86Sr isotopic, nannofossil and planktonic foraminiferal dating, Geological Magazine, 150, 333-359, 10.1017/S0016756812000465, 2013.

Miller, K. G., Wright, J. D., and Fairbanks, R. G.: Unlocking the Ice House: Oligocene-Miocene oxygen isotopes, eustasy, and margin erosion, Journal of Geophysical Research: Solid Earth, 96, 6829-6848, 10.1029/90JB02015@10.1002/(ISSN)2169-9356.LTSLC1, 1991a.

Miller, K. G., Feigenson, M. D., Wright, J. D., and Clement, B. M.: Miocene isotope reference section, Deep Sea Drilling Project Site 608: An evaluation of isotope and biostratigraphic resolution, Paleoceanography, 6, 10.1029/90PA01941, 1991b.

Miller, K. G., Browning, J. V., Schmelz, W. J., Kopp, R. E., Mountain, G. S., Wright, J. D., John Schmelz, W., Kopp, R. E., Mountain, G. S., and Wright, J. D.: Cenozoic sea-level and cryospheric evolution from deep-sea geochemical and continental margin records, Science Advances, 6, eaaz1346-eaaz1346, 10.1126/sciadv.aaz1346, 2020.

Miller, K. G., Kominz, M. A., Browning, J. V., Wright, J. D., Mountain, G. S., Katz, M. E., Sugarman, P. J., Cramer, B. S., Christie-Blick, N., and Pekar, S. F.: The phanerozoic record of global sea-level change, 10.1126/science.1116412, 2005.

Modestou, S. E., Leutert, T. J., Fernandez, A., Lear, C. H., and Meckler, A. N.: Warm middle Miocene Indian Ocean bottom water temperatures : comparison of clumped isotope and Mg / Ca based estimates, Paleoceanography and Paleoclimatology, 0-2, 10.1029/2020PA003927, 2020.

Moores, E. M. and Vine, F. J.: The Troodos Massif, Cyprus and other ophiolites as oceanic crust: evaluation and implications, Philosophical Transactions of the Royal Society of London. Series A, Mathematical and Physical Sciences, 268, 443-467, 1971.

Morse, T. J.: Biostratigraphical constraints (calcareous nannofossils) on the Late Cretaceous to Late Miocene evolution of SW Cyprus, 1996.

Necdet, M.: Kuzey Kıbrıs Jips Yatakları (Formation of Northern Cyprus gypsum), Unpublished PhD thesis, Çukurova University, 2002.

Ng, Z. L., Hernández-Molina, F. J., Duarte, D., Sierro, F. J., Ledesma, S., Rogerson, M., Llave, E., Roque, C., and Manar, M. A.: Latest Miocene restriction of the Mediterranean Outflow Water: a perspective from the Gulf of Cádiz, Geo-Marine Letters, 41, 1-17, 10.1007/S00367-021-00693-9/FIGURES/6, 2021.

Pantazis, T. M.: The geology and mineral resources of the Pharmakas-Kalavasos area, authority of the Republic of Cyprus1967.

Payne, A. S. and Robertson, A. H. F.: Neogene supra-subduction zone extension in the Polis graben system, west Cyprus, Journal - Geological Society (London), 152, 613-628, 10.1144/gsjgs.152.4.0613, 1995.

Pearson, P. N. and Palmer, M. R.: Atmospheric carbon dioxide concentrations over the past 60 million years, Nature, 406, 695-699, 10.1038/35021000, 2000.

https://doi.org/10.5194/egusphere-2025-442
Preprint. Discussion started: 12 February 2025

Pearson, P. N., Shackleton, N. J., and Hall, M. A.: Stable isotopic evidence for the sympatric divergence of Globigerinoides trilobus and Orbulina universa (planktonic foraminifera), Journal of the Geological Society, 154, 10.1144/gsjgs.154.2.0295, 1997.

Penttila, A.: Refining the timing of uplift in the northern margin of the Troodos Massif (Cyprus): Evidence from the Miocene sedimentary record, 2014.

Read, T. J.: The sedimentology of the Oligocene to Miocene Transition in the Limassol - Larnaca Area, Southern Cyprus, 1993.

Reghellin, D., Coxall, H. K., Dickens, G. R., and Backman, J.: Carbon and oxygen isotopes of bulk carbonate in sediment deposited beneath the eastern equatorial Pacific over the last 8 million years, Paleoceanography, 30, 1261-1286, 10.1002/2015PA002825, 2015.

Reidel, S.: Igneous Rock Associations 15. The Columbia River Basalt Group: A Flood Basalt Province in the Pacific Northwest, USA, Geoscience Canada, 42, 151-168, 2015.

Robertson, A. H. F.: Pelagic Chalks and Calciturbidites from the Lower Tertiary of the Troodos Massif, Cyprus, SEPM Journal of Sedimentary Research, Vol. 46, 10.1306/212f70bd-2b24-11d7-8648000102c1865d, 1976.

Robertson, A. H. F.: Tertiary uplift history of the Troodos massif, Cyprus, Bulletin of the Geological Society of America, 88, 1763-1772, 10.1130/0016-7606(1977)88<1763:TUHOTT>2.0.CO;2, 1977.

Robertson, A. H. F.: Tectonic evolution of Cyprus, Ophiolites and Oceanic Lithosphere. Proceedings of the International Symposium, Nicosia, Cyprus, 235-250,

Robertson, A. H. F.: Late Miocene paleoenvironments and tectonic setting of the southern margin of Cyprus and the Eratosthenes Seamount, Proceedings of the Ocean Drilling Program: Scientific Results, 160, 10.2973/odp.proc.sr.160.037.1998, 1998.

Robertson, A. H. F. and Hudson, J. D.: Cyprus umbers: Chemical precipitates on a Tethyan ocean ridge, Earth and Planetary Science Letters, 18, 10.1016/0012-821X(73)90039-3, 1973.

Robertson, A. H. F. and Parlak, O.: Eocene contractional deformation in the NW corner of the Arabian plate and its relation to Arabia-Eurasia collision in SE Türkiye, International Geology Review, 10.1080/00206814.2024.2400696, 2024.

Robertson, A. H. F. and Woodcock, N. H.: Mamonia Complex, southwest Cyprus: Evolution and emplacement of a Mesozoic continental margin, Bulletin of the Geological Society of America, 90, 10.1130/0016-7606(1979)90<651:MCSCEA>2.0.CO;2, 1979.

Robertson, A. H. F. and Woodcock, N. H.: The role of the Kyrenia Range Lineament, Cyprus, in the geological evolution of the eastern Mediterranean area, Philosophical Transactions of the Royal Society of London. Series A, Mathematical and Physical Sciences, 317, 141-177, 10.1098/RSTA.1986.0030, 1986.

Robertson, A. H. F. and Xenophontos, C.: Development of concepts concerning the Troodos ophiolite and adjacent units in Cyprus, Geological Society, London, Special Publications, 76, 85 LP-119, 10.1144/GSL.SP.1993.076.01.05, 1993.

Robertson, A. H. F., Parlak, O., and Ustaömer, T.: Overview of the Palaeozoic-Neogene evolution of Neotethys in the Eastern Mediterranean region (Southern Turkey, Cyprus, Syria), Petroleum Geoscience, 18, 10.1144/petgeo2011-091, 2012.

https://doi.org/10.5194/egusphere-2025-442
Preprint. Discussion started: 12 February 2025

Robertson, A. H. F., Clift, P. D., Degnan, P. J., and Jones, G.: Palaeogeographic and palaeotectonic evolution of the Eastern Mediterranean Neotethys, Palaeogeography, Palaeoclimatology, Palaeoecology, 87, 10.1016/0031-0182(91)90140-M, 1991.

Robertson, A. H. F., Eaton, S., Follows, E. J., and Payne, A. S.: Depositional processes and basin analysis of Messinian evaporites in Cyprus, Terra Nova, 7, 233-253, 10.1111/J.1365-3121.1995.TB00692.X, 1995a.

Robertson, A. H. F., McCay, G. A., Tasli, K., and Yildiz, A.: Eocene development of the northerly active continental margin of the Southern Neotethys in the Kyrenia Range, north Cyprus, Geological Magazine, 151, 10.1017/S0016756813000563, 2014.

Robertson, A. H. F., Necdet, M., Raffi, I., and Chen, G.: Early Messinian manganese deposition in NE Cyprus related to cyclical redox changes in a silled hemipelagic basin prior to the Mediterranean salinity crisis, Sedimentary Geology, 385, 126-148, 10.1016/J.SEDGEO.2019.03.009, 2019.

Robertson, A. H. F., Boulton, S. J., Tasli, K., Yildirim, N., Inan, N., Yildiz, A., and Parlak, O.: Late Cretaceous–Miocene sedimentary development of the Arabian continental margin in SE Turkey (Adıyaman region): Implications for regional palaeogeography and the closure history of Southern Neotethys, Journal of Asian Earth Sciences, 115, 571-616, 10.1016/J.JSEAES.2015.01.025, 2016.

Robertson, A. H. F., Kidd, R. B., Ivanov, M. K., Limonov, A. F., Woodside, J. M., Galindo-Zaldivar, J., and Nieto, L.: Eratosthenes Seamount: collisional processes in the easternmost Mediterranean in relation to the Plio-Quaternary uplift of southern Cyprus, Terra Nova, 7, 10.1111/j.1365-3121.1995.tb00693.x, 1995b.

Rouchy, J. M. and Caruso, A.: The Messinian salinity crisis in the Mediterranean basin: A reassessment of the data and an integrated scenario, 10.1016/j.sedgeo.2006.02.005, 2006.

Roveri, M., Flecker, R., Krijgsman, W., Lofi, J., Lugli, S., Manzi, V., Sierro, F. J., Bertini, A., Camerlenghi, A., De Lange, G., Govers, R., Hilgen, F. J., Hübscher, C., Meijer, P. T., and Stoica, M.: The Messinian Salinity Crisis: Past and future of a great challenge for marine sciences, Marine Geology, 352, 25-58, 10.1016/j.margeo.2014.02.002, 2014.

Ryan, W. B. F.: En: Messinian Events in the Mediterranean (CW Drooger, Ed.), 1973.

Sosdian, S. M. and Lear, C. H.: Initiation of the Western Pacific Warm Pool at the Middle Miocene Climate Transition?, Paleoceanography and Paleoclimatology, 35, 10.1029/2020pa003920, 2020.

Sosdian, S. M., Babila, T. L., Greenop, R., Foster, G. L., and Lear, C. H.: Ocean Carbon Storage across the middle Miocene: a new interpretation for the Monterey Event, Nature Communications 2020 11:1, 11, 1-11, 10.1038/s41467-019-13792-0, 2020.

Spezzaferri, S., Kucera, M., Pearson, P. N., Wade, B. S., Rappo, S., Poole, C. R., Morard, R., and Stalder, C.: Fossil and Genetic Evidence for the Polyphyletic Nature of the Planktonic Foraminifera "Globigerinoides", and Description of the New Genus Trilobatus, PLOS ONE, 10, e0128108-e0128108, 10.1371/JOURNAL.PONE.0128108, 2015.

Steinthorsdottir, M., Coxall, H. K., de Boer, A. M., Huber, M., Barbolini, N., Bradshaw, C. D., Burls, N. J., Feakins, S. J., Gasson, E., Henderiks, J., Holbourn, A. E., Kiel, S., Kohn, M. J., Knorr, G., Kürschner, W. M., Lear, C. H., Liebrand, D., Lunt, D. J., Mörs, T., Pearson, P. N., Pound, M. J., Stoll, H., and Strömberg, C. A. E.: The Miocene: The Future of the Past, Paleoceanography and Paleoclimatology, 36, e2020PA004037-e002020PA004037, 10.1029/2020PA004037, 2021.

Super, J. R., Thomas, E., Pagani, M., Huber, M., O'Brien, C. L., and Hull, P. M.: Miocene Evolution of North Atlantic Sea Surface Temperature, Paleoceanography and Paleoclimatology, 35, 10.1029/2019pa003748, 2020.

https://doi.org/10.5194/egusphere-2025-442
Preprint. Discussion started: 12 February 2025

Tanner, T., Hernández-Almeida, I., Drury, A. J., Guitián, J., and Stoll, H.: Decreasing Atmospheric CO2 During the Late Miocene Cooling, Paleoceanography and Paleoclimatology, 35, 10.1029/2020PA003925, 2020.

Torfstein, A. and Steinberg, J.: The Oligo–Miocene closure of the Tethys Ocean and evolution of the proto-Mediterranean Sea, Scientific Reports, 10, 10.1038/s41598-020-70652-4, 2020.

Tzanova, A., Herbert, T. D., and Peterson, L.: Cooling Mediterranean Sea surface temperatures during the Late Miocene provide a climate context for evolutionary transitions in Africa and Eurasia, Earth and Planetary Science Letters, 419, 71-80, https://doi.org/10.1016/j.epsl.2015.03.016, 2015.

Varol, B. and Atalar, C.: Messinian evaporites in the Mesaoria Basin, North Cyprus: facies and environmental interpretations, Carbonates and Evaporites, 32, 349-365, 10.1007/s13146-016-0311-8, 2017.

Vincent, E. and Berger, W. H.: Carbon dioxide and polar cooling in the Miocene: the Monterey hypothesis, The carbon cycle and atmospheric CO, 10.1029/gm032p0455, 1985.

Vincent, E., Killingley, J. S., and Berger, W. H.: The Magnetic Epoch-6 carbon shift: A change in the ocean's 13C/12C ratio 6.2 million years ago, Marine Micropaleontology, 5, 185-203, https://doi.org/10.1016/0377-8398(80)90010-9, 1980.

Wade, B. S. and Bown, P. R.: Calcareous nannofossils in extreme environments: The Messinian Salinity Crisis, Polemi Basin, Cyprus, Palaeogeography, Palaeoclimatology, Palaeoecology, 233, 10.1016/j.palaeo.2005.10.007, 2006.

Weijermars, R.: Neogene tectonics in the Western Mediterranean may have caused the Messinian salinity crisis and an associated glacial event, Tectonophysics, 148, 211-219, 10.1016/0040-1951(88)90129-1, 1988.

Westerhold, T., Bickert, T., and Röhl, U.: Middle to late Miocene oxygen isotope stratigraphy of ODP site 1085 (SE Atlantic): new constrains on Miocene climate variability and sea-level fluctuations, Palaeogeography, Palaeoclimatology, Palaeoecology, 217, 205-222, 10.1016/J.PALAEO.2004.12.001, 2005.

Westerhold, T., Marwan, N., Drury, A. J., Liebrand, D., Agnini, C., Anagnostou, E., Barnet, J. S. K., Bohaty, S. M., De Vleeschouwer, D., Florindo, F., Frederichs, T., Hodell, D. A., Holbourn, A. E., Kroon, D., Lauretano, V., Littler, K., Lourens, L. J., Lyle, M., Pälike, H., Röhl, U., Tian, J., Wilkens, R. H., Wilson, P. A., and Zachos, J. C.: An astronomically dated record of Earth's climate and its predictability over the last 66 million years, Science, 369, 1383-1388, 10.1126/SCIENCE.ABA6853/SUPPL_FILE/ABA6853_TABLES_S8_S34.XLSX, 2020.

Woodruff, F. and Savin, S. M.: δ13C values of Miocene Pacific benthic foraminifera: Correlations with sea level and biological productivity, Geology, 13, 119-122, 10.1130/0091-7613(1985)13<119:CVOMPB>2.0.CO;2, 1985.

Woodruff, F. and Savin, S. M.: Mid-Miocene isotope stratigraphy in the deep sea: High-resolution correlations, paleoclimatic cycles, and sediment preservation, Paleoceanography, 6, 10.1029/91PA02561, 1991.

You, Y.: Climate-model evaluation of the contribution of sea-surface temperature and carbon dioxide to the Middle Miocene Climate Optimum as a possible analogue of future climate change, Australian Journal of Earth Sciences, 57, 207-219, Pii 919320463

10.1080/08120090903521671, 2010.

You, Y., Huber, M., Müller, R. D., Poulsen, C. J., and Ribbe, J.: Simulation of the Middle Miocene Climate Optimum, Geophysical Research Letters, 36, 4702-4702, 10.1029/2008GL036571, 2009.

https://doi.org/10.5194/egusphere-2025-442
Preprint. Discussion started: 12 February 2025

Zachos, J. C., Dickens, G. R., and Zeebe, R. E.: An early Cenozoic perspective on greenhouse warming and carbon-cycle dynamics, Nature 2008 451:7176, 451, 279-283, 10.1038/nature06588, 2008.

Zachos, J. C., Pagani, H., Sloan, L., Thomas, E., and Billups, K.: Trends, rhythms, and aberrations in global climate 65 Ma to present, 10.1126/science.1059412, 2001.

Zhang, Y. G., Pagani, M., Liu, Z., Bohaty, S. M., and DeConto, R.: A 40-million-year history of atmospheric CO ₂, Philosophical Transactions of the Royal Society A: Mathematical, Physical and Engineering Sciences, 371, 20130096-20130096, 10.1098/rsta.2013.0096, 2013.